On the Residual Stress Measurements in Y-Based Superconductor

by

Shakir Nasir Al-Faer

A Thesis Presented to the

FACULTY OF THE COLLEGE OF GRADUATE STUDIES

KING FAHD UNIVERSITY OF PETROLEUM & MINERALS

DHAHRAN, SAUDI ARABIA

In Partial Fulfillment of the
Requirements for the Degree of

MASTER OF SCIENCE

In

PHYSICS

June, 1997

INFORMATION TO USERS

This manuscript has been reproduced from the microfilm master. UMI films the text directly from the original or copy submitted. Thus, some thesis and dissertation copies are in typewriter face, while others may be from any type of computer printer.

The quality of this reproduction is dependent upon the quality of the copy submitted. Broken or indistinct print, colored or poor quality illustrations and photographs, print bleedthrough, substandard margins, and improper alignment can adversely affect reproduction.

In the unlikely event that the author did not send UMI a complete manuscript and there are missing pages, these will be noted. Also, if unauthorized copyright material had to be removed, a note will indicate the deletion.

Oversize materials (e.g., maps, drawings, charts) are reproduced by sectioning the original, beginning at the upper left-hand corner and continuing from left to right in equal sections with small overlaps. Each original is also photographed in one exposure and is included in reduced form at the back of the book.

Photographs included in the original manuscript have been reproduced xerographically in this copy. Higher quality 6" x 9" black and white photographic prints are available for any photographs or illustrations appearing in this copy for an additional charge. Contact UMI directly to order.

UMI

A Bell & Howell Information Company
300 North Zeeb Road, Ann Arbor MI 48106-1346 USA
313/761-4700 800/521-0600

ON THE RESIDUAL STRESS MEASUREMENTS IN Y-BASED SUPERCONDUCTOR

BY

SHAKIR NASIR ALFAER

A Thesis Presented to the

FACULTY OF THE COLLEGE OF GRADUATE STUDIES

KING FAHD UNIVERSITY OF PETROLEUM & MINERALS

DHAHRAN, SAUDI ARABIA

In Partial Fulfillment of the
Requirements for the Degree of

MASTER OF SCIENCE
In
PHYSICS

JUNE 1997

KING FAHD UNIVERSITY OF PETROLEUM AND MINERALS

DHAHRAN 31261, SAUDI ARABIA

COLLEGE OF GRADUATE STUDIES

This thesis, written by Shakir Nasir Alfaer **under the direction of his Thesis Advisor and approved by his Thesis Committee, has been presented to and accepted by the Dean of the College of Graduate Studies, in partial fulfillment of the requirements for the degree of MASTER OF SCIENCE IN PHYSICS.**

Thesis Committee:

Dr. Khalil A. Ziq
Chairman of the Thesis Committee

Dr N. Hamdan
Member

Dr. John Shirokoff
Member

Dr. A. S. Al-Harthi
Member

Department Chairman

Dean, College of Graduate Studies

30-12-98
Date

Acknowledgment

Praise to Allah the Lord of the world and peace and plessing be upon Prophet Mohammad.

I would like to express my deep gratitude and appreciation to my thesis advisor, Dr. Khalil A. Ziq for his limitless patience, encouragement and support. I wish also to express my gratefulness to my thesis committee; Dr. N. M. Hamdan, Dr Abdulaziz Salem Al-Harthi and in particular Dr. J. W. Shirokoff for their valuable suggestions and helpful remarks and their kind cooperation.

I would like to express my appreciation to my undergraduate advisor Dr. Adnan Al-Aswad for his encouragement, support and valuable advises

I would like to thank my family and friends specially my brother Mansour and my friend A. Aljalal for their encouragement and support.

I would like to express my sincere thanks to my wife for her encouragement and support.

Finally, I acknowledge King Fahd University of Petroleum and Minerals and the Physics Department for supporting this research.

ABSTRACT

XRD and residual stress ($\sim \sin^2\psi$) measurements were carried out on $YBa_2Cu_3O_x$ superconductor with varying oxygen stoichiometry $x = 6.32$ to 7.

Using published data for c-axis, T_c and oxygen content it was found that the measured c-axis varies linearly with and is sensitive to variation of oxygen content and T_c. Variation of a and b parameters with oxygen content revealed a transition from orthorhombic to tetragonal at 6.48. Orthorhombicity and volume of the unit cell were plotted against oxygen content and an unexpected volume contraction of the unit cell was observed. This was discussed in terms of energetically favored filling of oxygen sites. Slopes of the strain versus $\sin^2\psi$ which is proportional to the residual stress, were plotted against oxygen content for certain reflections (006) and (115), for example. Different behaviors were observed and are attributed to a c-axis compressional stress increasing with oxygen content and an overall tensile residual stress in the ab-plane is also increasing oxygen content. Both effects reach saturation near fully oxygenated state $x \approx 7$. This explains the anomalous very small hydrostatic pressure effect on T_c for fully oxygenated $YBa_2Cu_3O_x$ ($x \approx 7$) compared to a relatively high effect for oxygen deficient material. Similar results were observed for the oxygen disorder effect. Changes in T_c for disordered material is attributed to changes in the residual stress induced by disorder phenomena.

الخلاصة

تعنى هذه الأطروحة بدراسة طريقة قياس الإجهاد المتبقي باستخدام تشتت الأشعة السينية (XRD) للمـــواد المفرطة التوصيل من نوع $Y_1 Ba_2 Cu_3 O_x$ يحتوي على نسب مختلفة من الأكسجين بين ٦.٣٢ و ٧ .

أظهرت النتائج أن الأبعاد البلورية (a, b, c) تتغير بتغير نسبة الأكسجين. ولوحظ أن البعد (c) يتغير بشكل خطي مع تغير نسبة الأكسجين متفقا مع النتائج المنشورة في هذا المجال وأظهر التغير في كل من a و b أن الانتقال التركيبي من طور orthorhombic إلى طور tetragonal يحصل عند نسبة أكســـجين قدرهـــا ٦.٤٨.

هذا وقد تم حساب الانحراف عن الطور orthorhombic وحجم وحدة البناء البلـــوري أثنـــاء تغـير نســبة الأكسجين

وأظهرت النتائج أن التغير في الحجم كان غير متوقع ويمكن رده إلى أن ذرات الأكســـجين تشـــغل المواقـــع البلورية حسب الطاقة المفضلة (المناسبة).

مكننتا هذه النتائج من تحديد الإجهاد المتبقي لنسب مختلفة من الأكسجين من خلال تمثيل ميل منحنيات الشد مع $\sin^2 \psi$ للمستويات (006) و (115) على سبيل المثال. لاحظنا تغيرات مختلفة لسلوك منحنيـــات الإجـــهاد المتبقي حيث كان الإجهاد المتبقي في البعد (c) جهدا انضغاطيا يزداد بزيادة نسبة الأكسجين في حيـــن كـــان الإجهاد في مستوى (ab) جهدا شديا يزداد أيضا بزيادة نسبة الأكسجين في هذه المواد المفرطة الإيصاليـــة . كما وجدنا أن كلا الجهدين يقارب حالة الإشباع عندما تصل نسبة الأكسجين قريبا من ٧.

تفسر نتائجنا بعض الظواهر الغريبة والتي تتعلق بالاثر القليل للضغـــط الخـــارجي علـــى درجـــات الحـــرارة الانتقالية عندما تكون نسبة الأكسجين قرب ٧ مقارنة بالنسب الأخرى (اقل من ٧).

أجرينا دراسة مبدئية لأثر عدم الانتظام في شغل مواقع الأكسجين ، ودلت هذه الدراسة أن هناك تغير واضـــح في قيم الإجهاد بالرغم من عدم تغير نسبة الأكسجين.

Contents

List of Figures

List of Tables

Chapter 1

Introduction

In 1908 Heike Kamerlingh Onnes, in The Netherlands succeeded in liquefying helium at its boiling temperature of 4.15 **K**, the lowest achieved temperature of a substance at that time [49].This achievement provided Onnes and his assistants with the tool to investigate the transport properties of materials at extremely low temperatures. In 1911, Onnes discovered one of the superconducting properties while measuring the electrical resistance of mercury near liquid helium temperature (4.2 K) [49]. He found out that the resistivity drops sharply and suddenly at 4 K to about 10^{-4} of its original value, unlike what is expected classically [1], [49]. This characterizing transition temperature was called the *critical temperature or the superconducting transition temperature* T_c, below which materials become perfect conductors.

Perfect conductivity [49] is the first striking feature of Superconductors. For perfect conductors, if the applied magnetic field H is increased from zero up to a certain critical field H_C, it induces surface current which in turn produces a field that opposes the applied field. The field will be excluded from the interior of the sample,

and the net internal field will be cancelled out, and $B = 0$, this is known as perfect diamagnetism. Up to this point the superconductor behaves exactly like a perfect conductor. For $H \geq H_C$ the superconductor becomes normal and field penetrates the sample completely and $B = H_C$ inside. If the superconductor were a perfect conductor the flux will be **trapped in** as the field is lowered below H_C, which is not the case for an ideal superconductor, for which the field will be **expelled again** from the sample. This reversible process of expulsion of the field out of the sample interior as long as it is below critical value H_C *(Perfect diamagnetism)* is called the Meissner effect after Meissner and Ochsenfeld who discovered it in 1933 [9], [52]. *Perfect diamagnetism* is the second characterizing feature of superconductivity [51].

For practical applications of superconducting materials, the critical current density ($\mathbf{J_c}$) is an important characterizing property of Superconductors, because when the applied current exceeds $\mathbf{J_c}$, this causes the material to lose its superconducting properties. In other words, $\mathbf{J_c}$ is the maximum current density which the material can carry without dissipation [51].

The critical field (H_C) is related to the difference of free energy between the normal and the superconducting reversible phases through the equation [51]:

$$\frac{H_C^2(T)}{8\pi} = F_n(T) - F_s(T) \tag{1.1}$$

Experimentally, H_C can be evaluated from the reversible magnetization or specific heat measurements. It was found empirically that H_C has a parabolic variation with T (Fig. 1.1), i.e.

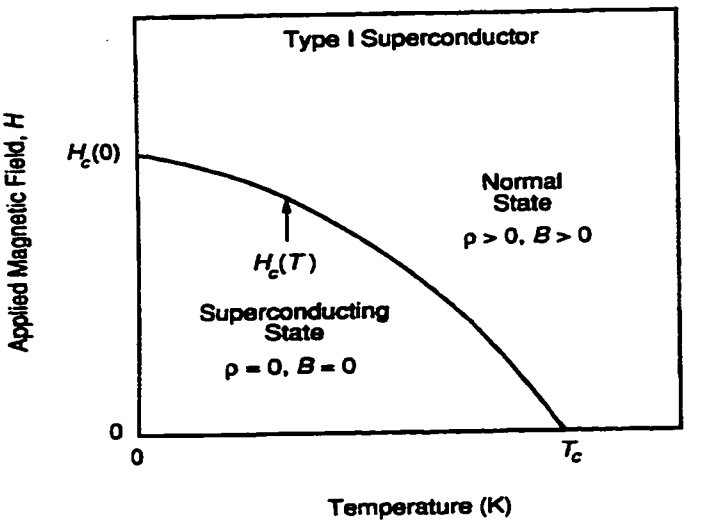

Figure 1.1: *The two possible states of Type I superconductor. Both the applied magnetic field and temperature must be below critical levels or otherwise a superconductor will turn to the normal state [after Doss, [11]].*

$$H_C(T) = H_C(0)\left[1 - \left(\frac{T}{T_C}\right)^2\right] \tag{1.2}$$

The above two basic properties of superconductivity, namely; *perfect conductivity and perfect diamagnetism (i.e. Meissner effect)* were well described by the London brothers in 1935 with the two equations [45], [7]:

$$\mathbf{E} = \frac{\partial}{\partial t}(\Lambda \mathbf{J}_S) \tag{1.3}$$

$$\mathbf{H} = -c\nabla \times (\Lambda \mathbf{J}_S) \tag{1.4}$$

where

$$\Lambda = \frac{4\pi\lambda_L^2}{c^2} = \frac{m}{n_s e^2}$$

and

$$\lambda_L^2 = \frac{mc^2}{4\pi n_s e^2} \tag{1.5}$$

where λ_L is the *London penetration depth* for the magnitude that an external magnetic flux can penetrate into a superconducting material [45], [11]. The transition to superconducting state can be seen as a discontinuity in the electronic specific heat curve at T_C. Well below T_C, the electronic specific heat is dominated by an exponential dependence $e^{-\frac{\Delta}{k_B T}}$, while above T_C, the normal state electronic specific heat is linear in T($\sim \gamma T$). Electromagnetic absorption measurements were interpreted in BCS theory quite convincingly in terms of the energy gap of three to four times of kT_c [11].

Ginsburg and Landau proposed their phenomenological GL-theory of superconductivity in 1950 which can treat two features which were beyond the scope of the London theory [9]:

1. Nonlinear effects in fields strong enough to change n_s.

2. Spatial variations of n_s.

GL-theory predicts that the temperature dependent coherence length $\xi(T)$ diverges as $(T_c - T)^{-\frac{1}{2}}$ near T_c. Moreover, the ratio of the characteristic lengths ξ_{GL} ($\xi(T)$)and λ defines the important GL parameter κ such that [52]

$$\kappa = \frac{\lambda}{\xi_{GL}} \tag{1.6}$$

One of the important concepts of superconductivity is the concept of *surface energy*. This concept was first introduced by London who noted that the total exclusion

of the field would not lead to the state of the lowest energy unless a boundary energy exists between the normal and the superconducting regions. This energy is called the surface energy [9], [52].

Surface energy and the value of κ were the basis of the classification of superconducting materials by Abrikosov in 1952 [9]. He showed that the breakpoint for zero surface energy is at $\kappa = \frac{1}{\sqrt{2}}$. This classification may be made as follows:

- Type I superconductors: $\kappa < \frac{1}{\sqrt{2}}$, yields positive surface energy and occurs in most elemental superconductors.

- Type II superconductors: $\kappa > \frac{1}{\sqrt{2}}$, yields negative surface energy like Nb, V, Ta high T_c superconductors and superconducting alloys [9], [52].

1.1 High T_C Superconductors (HTSC)

In 1986 a new class of superconductors was discovered by Bednorz and Muller [2] that has a transition temperature T_C in excess of 30K [4]. As a result, a new division in superconductivity was commonly used :

- Conventional Superconductors; All known superconducting materials (elemental, alloys, etc..) with the highest $T_C \approx 23.2$ K of Nb_3Ge

- High T_C Superconductors; All are type-II alloys, ceramic, oxides discovered after 1986 and commonly have transition temperatures above 25 K [4].

These HTSCs are generally divided into four main groups :

- Y-based copper oxide HTSC with general formula $Y(R)Ba_2Cu_3O_{7-\delta}$ was discovered with a transition temperature in the 90 K range, which is well above liquid nitrogen temperature (77.3 K). Of particular interest on which this work will focus on is the study of the compound $Y_1Ba_2Cu_3O_{7-\delta}$ [7], [15], [23].

- Bi- based copper oxide HTSC with the general formula $((BiO)_2\, Sr_2Ca_{n-1}Cu_nO_{2n+2})$ where n is the number of Cu_2 layers and T_c around 110 K for $n = 3$. This was discovered in 1988 [11], [34].

- T*l*-based copper oxide HTSC with general formula $((TlO)_m\, Ba_2Ca_{n-1}Cu_nO_{2n+2})$ with $m = 1, 2$ and $n = 1, 2, 3$. T_c is about 125 K for $m = 2$ and $n = 3$ and was also discovered in 1988 [11], [34].

- Hg-based copper oxide HTSC with the general formula $((HgO)\, Ba_2Ca_{n-1}Cu_nO_{2n+1+\delta})$ with T_c above 130 K, was discovered in 1993 [13], [16], [22].

1.1.1 Common Properties of HTSC's

High Temperature Superconductors are ceramic oxides. They are brittle and inflexible materials. The oxygen content and disorder have pronounced effect on the superconducting and normal state properties of HTSC's [4], [32]. They share the following common properties :

1. Anisotropic crystal structure ; Electrical and magnetic properties behaves differently along the crystalline direction [40].

2. Electron or hole doping of the Cu-O planes effects their normal and superconducting properties [4], [22], [40].

3. Many HTSC have a very high upper critical field ($\sim 100\ Tesla$) and low J_c ($10^4 - 10^5 \text{A cm}^{-2}$) at 4 K. This behavior is mainly due to grain boundary, weak links and weak flux pinning [32], [40].

4. These materials have extremely high T_c which exceeds the BCS theory limit 40 K [40], [42].

5. They are all type-II superconductors with a very large Ginsburg-Landau (GL) parameter κ and κ is anisotropic because ξ is very small ($\ll \lambda$) and it is also anisotropic [40].

1.1.2 Differences and Similarities Between Conventional Superconductors and HTSC's

Differences

HTSC's properties differ from those of conventional superconductors in many ways. The main differences are listed below.

1. One of the main differences is that the superconducting coherence length ξ is extremely short compared to low temperature conventional superconductors (LTSC). The Bardeen Cooper Schrieffer (BCS) theory for the intrinsic temperature independent coherence length is given in the following relation:

$$\xi_0 = 0.18\frac{\hbar v_F}{k_B T_c} \tag{1.7}$$

Therefore high T_c leads to small ξ_0, for $Y_1Ba_2Cu_3O_{7-\delta}$, ξ_0 is at least one tenth ξ_0 for Nb. Low carrier density N is also a source of small ξ_0, since v_F (Fermi velocity) is proportional to $N^{\frac{1}{3}}$. The other temperature dependent coherence length which is known as the Ginsburg-Landau coherence length ξ_{GL}, which determines the size of the fluxoid, and it is related to the upper critical field(H_{c_2}) by the relation:

$$\frac{\phi_0}{2\pi\xi_{GL}^2} = \mu_0 H_{c_2} \tag{1.8}$$

Therefore, H_{c_2} $(HTSC) \gg H_{c_2}$ $(LTSC)$. The parameters ξ_{GL} and ξ_0 are closely related through the relation:

$$\xi_{GL} = 0.74\xi_0 \left\{1 - \left(\frac{T}{T_c}\right)\right\}^{-\frac{1}{2}} \tag{1.9}$$

For $T \ll T_c$ ξ_{GL} is typically between 0.5 and 30 Å [7], [32], [39], [40]. Moreover, Ginsburg-Landau constant $\kappa(HTSC) \gg \kappa(LTSC)$. Short coherence length of HTSC's manifests itself in fluctuation effects observed in specific heat, conductivity and magnetic susceptibility [32].

2. Various experimental results have indicated that the wave function of the paired carriers has a d-symmetry [42], unlike what is commonly known for LTSC, where the wave function of the paired carriers has an s-symmetry [40]. This result means that **BCS** model for conventional superconductors is no longer valid for high-temperature superconductors [42].

3. It seems that the crystalline structure of HTSC has a lower symmetry than the crystalline structure of conventional superconductors [11].

Similarities

1. Superconducting states are made up of paired carriers [4].

2. Both superconductors have an energy gap. However, for HTSC's the energy gap is probably anisotropic and lies in the range $3.5k_BT_c$ to $8k_BT_c$ which is larger than the isotropic **BCS** value of $3.54k_BT_c$ [4], [40].

3. Both have a jump in their heat capacity at $T=T_c$ [40].

4. No linear term in heat capacity has been observed at low temperatures. This is a characteristic feature of normal metals and conventional superconductors [40].

5. T_c is a non-monotonic function of carriers concentration n_c in HTSC's. The transition temperature is maximum for optimal of n_c [40].

6. Josephson tunneling and the vortex structure in HTSC are similar to what is observed in conventional type II superconducting materials [4].

1.1.3 Crystal Structure of HTSC's

High-T_c oxides are multinary compounds that may contain up to five or even more different elements [50]. The crystalline structures are referred to as perovskites that may contain up to sixteen symmetry independent atom sites [54]. The simple perovskites (isotropic structure) are cubic in structure with simple chemical formula ABX_3, where metal A and the non-metal X are arranged in a cubic layer sequence. An example of an ideal perovskite is $CaTiO_3$. The structure of High-T_c oxides are also

complex variations from the ideal form, and often referred to as defected perovskite. Variations and structural defect are caused by mixing between A and B cations, non-stoichiometry, octahedral tilting, twinning, impurities or combinations of the above. These variations lead to marked differences in magnetic, electrical, mechanical, and optical properties, including anisotropy [11].

The crystal structure of high-temperature superconductors contains layers composed of Cu-O_2 planes and separated from each other by planes of other oxides and rare earths [4]. The Cu-O_2 planes are found to play a vital role in superconductivity and charge transport in HTSC. In this thesis, we will study the effect of changing the oxygen content in Cu-O_2 planes and in Cu-O chains in YBCO where oxygen is believed to play an important role [4], [18], [27].

An alternative way to describe high T_c superconductors is by an intergrowth of peroskites and rock-salt like slabs with a specific sequence for a given type of HTSC structure [33].

1.1.4 Crystal Structure of YBCO High-T_C Material

The crystal structure of YBCO is shown in Fig(1.2). It is generated by stacking three perovskite ABO_3 unit cells one on top of the other with the A site alternating between Y and Ba with cation ordering —Y—Ba—Ba—Y—Ba—Ba—. There are 9 possible anion i.e. oxygen sites in this tripled perovskite unit cell [3]. Upon the removal of up to three oxygen atoms we end up with layers stacking as —Y—CuO_2— BaO—CuO— BaO—CuO_2—Y— and the chemical formula is given as $Y_1Ba_2Cu_3O_{7-\delta}$

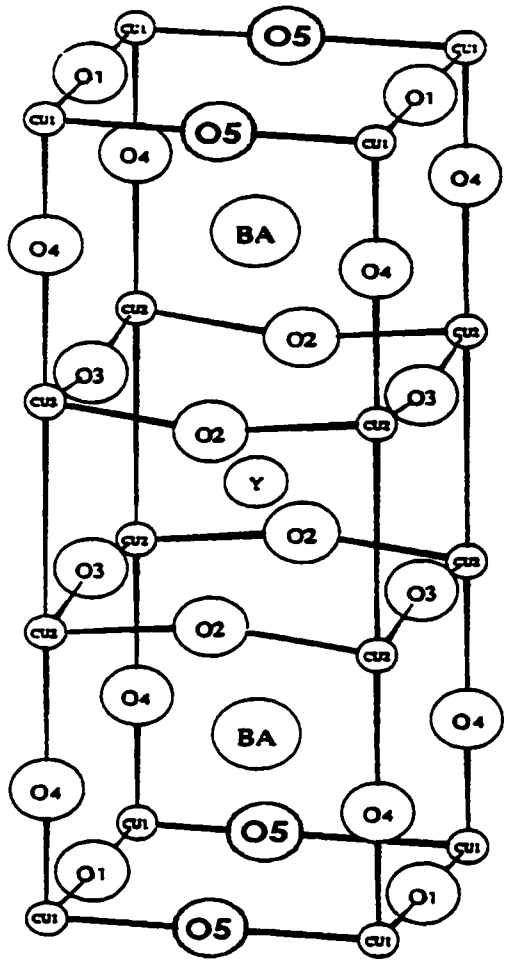

Figure 1.2: *The crystal structure of* $YBa_2Cu_3O_{7-\delta}$. *O(1) site is along* **b** *axis and O(5) site is along* **a** *axis.*

[54]. The smaller size of the middle Y cation and the removal of oxygen atoms on the edges of the middle cell result in compression (internal stress) of the middle cell in the **c** direction [7]. As we can see from Fig(1.2), between the two immediately adjacent CuO_2 plane (*conduction planes*) lies the Y atom plane . This CuO_2 pair of planes is separated from the next pair by three metal-O planes. These planes are called the "isolation planes" or "charge reservoirs" [4]. The crystal structure changes from *tetragonal* to *orthorhombic* and the material changes from insulator to superconductor as a result of the changes of the oxygen stoichiometry. Oxygen content x $(= 7 - \delta)$can be changed from a relatively sharp lower limiting value $x = 6$, i.e. $(\delta = 1)$ to a relatively diffuse upper limiting value $x = 7$, i.e. $(\delta = 0)$.

Oxygen content with $x > 7$ can be achieved by cation substitution. The transition temperature T_c decreases with decreasing the oxygen content in a manner shown in Figs (1.3) and (1.4). The Figures reveals a slight decrease in T_c with deceasing

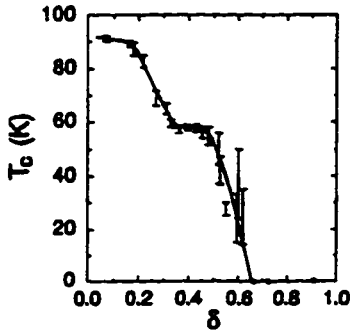

Figure 1.3: *Superconducting transition temperature T_c as a function of δ for samples of $YBa_2Cu_3O_{7-\delta}$ annealed at 520 °C and quenched into liquid nitrogen from various oxygen partial pressure [after Jergensen et al., [20]].*

x for $7 > x > 6.8$, a rapid decrease for $6.8 > x > 6.7$, remains almost constant at

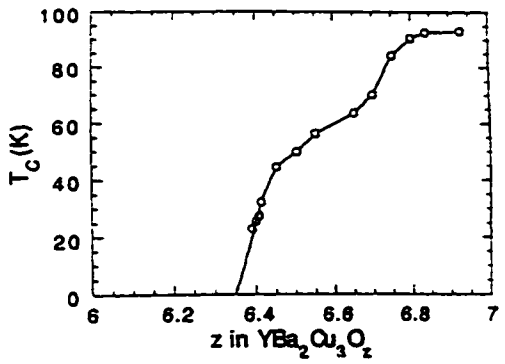

Figure 1.4: *Superconducting transition temperature T_c as a function of oxygen content $x = 7 - \delta$ in $YBa_2Cu_3O_{7-\delta}$ [after Yang, [53]].*

the value of 60 **K** for $6.7 > x > 6.5$ and drops sharply from 60 **K** to 0 **K** for $6.5 > x > 6.4$. Structural changes are also associated with vacancies produced by removing oxygen atoms from the structure. Eventually an orthorhombic to tetragonal phase transformation occurs in the region from $6.4 > x > 6$ in which the material behaves as an antiferromagnetic insulator [34], [53]. As the oxygen content decreases, the lattice parameters start changing, thus producing strains on the structure. It is expected that the orthorhombicity factor changes with changing oxygen content. This is a direct measure of the strain and will be treated in chapter 2 and 4. Oxygen contents mentioned above are reported by most of the studies for the distinction between different regions in the structure. However, some studies give different numbers [3], [4], [34], [53], [54] (a 60 K region extends between $x = 6.28$ and $x = 6.61$ [4]). These differences can be attributed to inaccurate determination of oxygen content, sample history (the exact stoichiometries where the transitions occur depend sensitively on material preparation processing [25]) and different methods used to estimate T_c(onset,

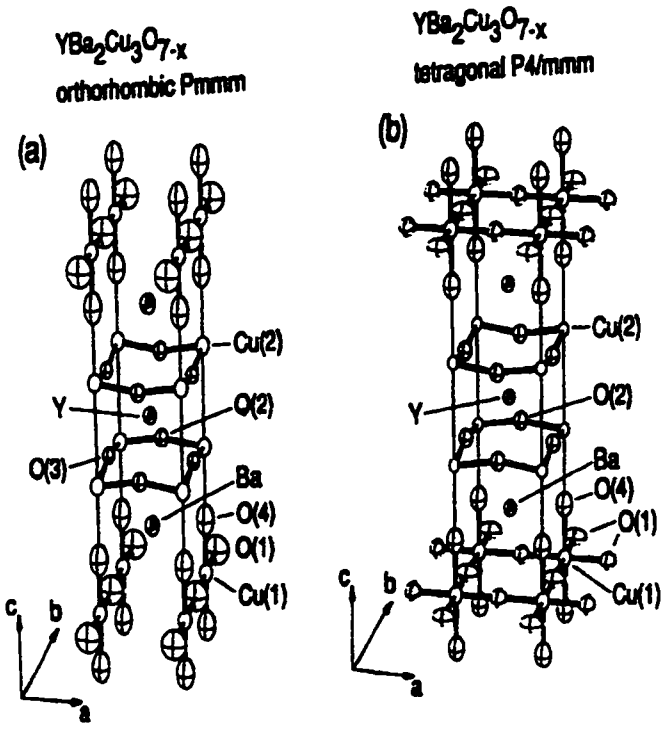

Figure 1.5: *(a) Orthorhombic and (b) tetragonal structure of* $YBa_2Cu_3O_{7-\delta}$. *In the tetragonal structure, the different atom symbol for O(1) site is used to indicate that this site is not fully occupied [after Jergensen et al.,* [20]].

midpoint etc). There are at least two plateaus namely; so called 60 K ($6.7 > x > 6.5$) and 90 K ($7 > x > 6.8$) plateaus [25] which are associated with ortho I and ortho II superstructures. Other phases or superstructures (e.g. ortho III, ortho V) are also reported [34], [53], [39].

Oddly, some high temperature quenching studies show no pronounced plateau behavior but rather a fairly smooth decrease of T_c with increasing x [17], [14].

Orthorhombic Structure

Variances in oxygen content due to different heat treatment can account for differences in unit cell dimensions and atomic cell reported [24], [3]. Differences in the stoichiometric ratio in YBCO may also affect the lattice parameters and the observed discrepancies reported in the literature. For the oxygen content $x \sim 7$ (i.e., $\delta \sim 0$), at room temperature, the structure is orthorhombic (ortho I) with lattice parameters $a = 3.816\,(2)$ Å, $b\,(\approx a) = 3.892\,(2)$ Å and $c\,(\approx 3a) = 11.682\,(9)$ Å [21]. The space group is Pmmm and the point group is 2/mmm of order 8 [47]. The yttrium site has eight nearest neighbor oxygen atoms in a nearly cubic arrangement (eight fold oxygen coordination), barium site with ten oxygen nearest neighbors (ten fold oxygen coordination) in a truncated cube-octahedral arrangement. There are two distinct copper sites, i.e. Cu(1) site "the linear chain site" (because it is positioned on the linear O(1) −Cu(1) −O(1) chains that run along the **b** direction) with fourfold coordination and a square-planar arrangement with respect to oxygen atoms. The Cu(2) site (Cu-plane) is with fourfold coordination (four oxygen nearest neighbors) and with square-pyramidal arrangement with respect to the oxygen atoms. There are also four distinct oxygen sites (O(1) ,O(2) ,O(3) ,O(4)) in the structure .Three oxygen sites (O(2) ,O(3) ,O(4)) are fully and one (O(1)) is partially occupied (at $x = 7$ all available O(1) sites are occupied(all chains filled)) as shown in Fig 1.5 [34], [39], [54].

Tetragonal Structure

For low oxygen content $x \sim 6$ (i.e., $\delta \sim 1$), at room temperature, the structure is tetragonal with lattice parameters $a = b = 3.8570\,(1)$ Å, $c\,(\approx 3a) = 11.8194\,(3)$ Å [3]. The space group is P4/mmm and the point group 4/m 2/m 2/m of order 16 [47]. The structure contains another oxygen O(5) site which is empty at $x = 6$ (chains do not exist). As x increases O(1) and O(5) are equally occupied. At a critical value of x ($6.34 < x < 6.4$ [3]), O(5) becomes empty again. The coordination number of Cu(1) site is reduced to two as shown in Fig (1.5).

Phase Transition and Stoichiometry Effect

At $x = 6$, the O(1) and O(5) sites are empty and the **a** and **b** lattice parameters are equal and hence the orthorhombic ratio or strain $e = 0$ $\left(e = 2\frac{(b-a)}{(b+a)}\right)$ [54]. As x increases O(1) and O(5) are equally occupied until x reaches a critical value $(6.34 < x < 6.4)$ [3] were a structural transformation (phase transition) from tetragonal to orthorhombic occurs, with only O(1) site occupied. As we go across the transition region, the parameter **b** increases and at the same time parameter **a** and **c** decreases resulting in a decrease in the volume of the cell. Also, the **c** parameter and the volume of unit cell is known to decrease. Further increasing of the value of x will result in an increased occupancy of O(1) site. At $x = 7$, all the available O(1) sites are occupied [14], [20], [24], [25], [30], [53].

Upon decreasing the oxygen content, the anisotropy of YBCO material deceases resulting in a lower dimensionality (from three to two dimensional system). Penetra-

tion depth anisotropy parameter $\gamma = \frac{\lambda_c}{\lambda_{ab}}$ can be taken as a measure of anisotropy. The coherence length ξ and penetration depth λ and the Ginzburg-Landau parameter changes as the oxygen content changes. Both parameters ξ_{ab} and λ_{ab} increase as the oxygen content is decreased. Also, the critical temperature decreases as the oxygen content is decreased [39].

The orthorhombic to tetragonal phase transition is an order-disorder phase transition. Here, the oxygen arrangement changes from fully ordered at room temperature to partially ordered at high temperature in the orthorhombic phase, to completely disordered (at higher temperatures) in the tetragonal phase [25], [39], [10].

Order Disorder Phenomena

Usually solids are disordered at high temperatures and ordered at low temperatures. "Ordered" means that the lattice sites can be arranged into sublattices. In a disordered state, no such grouping is present, each sublattice is being occupied by various atoms at random [8].

There exist three kind of disordering:

1. Positional disordering.

2. Orientational disordering.

3. Disordering linked to the electronic and nuclear state, For a detailed study of this phenomena see reference [53].

In HTSC, the positional oxygen order disorder effect is of special importance. For example, the superconducting and normal properties of $Y_1Ba_2Cu_3O_{7+\delta}$ does not de-

pend only on oxygen stoichiometry but also on the degree of ordering. Two types of ordering are commonly identified, long range and short range ordering. The first, manifests itself in the appearance of what is called, superlattice or superstructure, reflections in the diffraction patterns. Short range ordering does not produce superlattices but rather affects the background scattering intensity [10], [53].

Oxygen disorder can be achieved by low temperature annealing of samples with defined oxygen content are usually annealed at about 200 $^{\circ}c$ then quenched in liquid nitrogen to freeze the 200$^{\circ}c$ state. Although the oxygen content is fixed, T_c may change dramatically depending on the degree of oxygen disorder [53]. In this process some of the O(1) site atoms will occupy vacant nearby sites and a change in T_c should be expected. Conversely, as more vacancies are available a large degree of disorder is introduced [39], [10], [53].

Therefore, one should treat the x-T_c phase diagram with caution, as the degree of oxygen disorder depends on many factors such as annealing temperature quenching time and the oxygen content itself. For more details on the ordering problem see references [39], [47], [53].

Chapter 2

Residual Stress and Pressure Effect

Interests in high-T_c superconductors were mainly driven by hopes and dreams of scientists to produce a room temperature SC. By the late eighties, two main schemes could recognized. First, to search for trends or systematics in the variation of transition temperature T_c with parameters such as the concentration n of charge carriers in the CuO_2 plane or the applied pressure P [12]. This was first driven in part by the observation of the pressure dependence of T_c in classical SC, and to look for the effect of **internal** (chemical) pressure. Second, almost random substitution of all elements of the periodic table in HTSC and looking for the corresponding effects on T_c and other properties. The outreach of the second trend was to change the electronic structure by doping [29].

2.1 Pressure Effect

For conventional superconductors, variations of T_c with pressure can be accounted for using **BCS** theory of superconductivity. According to **BCS** theory, pressure affects the lattice spacing and eventually the phonon spectrum, thus affecting the phonon mediated electron-electron interaction [7], [50]. However, the shift in transition temperature T_c with pressure for HTSC is one or two orders of magnitude higher than in most conventional superconductors [37]. Ultrasound measurements [5], [6] indicate that the effect of pressure on transition temperature in many HTSC like YBCO is less than that of Hg-based HTSC's where it is quite large. One of the milestones of the high-T_c superconductivity was the important observation by Chu et al. [15] where it was found that $\frac{dT_c}{dP}$ was positive and very large in $(La,Ba)_2CuO_4$ under **hydrostatic pressure** [15]. This observation led them to the suggestion of the possibility of greatly increasing T_c by inducing **internal pressure** which can be generated by a large A-B size difference in ABCuO compound. Soon after their predictions, their hopes became evident and two high T_c superconductors which have T_c above liquid nitrogen temperature were discovered namely; $Y_1Ba_2Cu_3O_7$ ($T_c = 93$ **K**) and $La(La_{2-x},Ba_x)Cu_3O_7$ ($T_c = 80$ **K**) [23], [50]. Superconductivity above 150 **K** may be achieved in Hg-1223 at ambient pressure by suitable forms of chemical substitution as it was predicted by Chu et al. [16] after they found a strong T_c dependence on pressure (T_c up to 153 **K** at 150 kbar) [16].

In general, $\frac{dT_c}{dP}$ is always positive and rather large in most hole-doped cuprate superconductors, with a characteristic difference between relatively low and high T_c

values increasing pressure. However, there are some hole-doped compounds which show a negative coefficient, and other hole-doped compounds which change from positive to negative values with increasing pressure with a maximum at T_c. On the other hand, electron doped compounds (e.g.,$Nd_{2-x}Ce_xCuO_{4-y}$) show almost no response to pressure [44], [38].

Pressure affects many of the physical properties of materials by basically reduceing the value of lattice parameters. For HTSC, it increases the ratio of Cu^{3+} to Cu^{2+} [50], [11] and may induce oxygen ordering in many high T_c cuprates [31], [12]. The application of pressure generally increases T_c of underdoped layered cuprates, with $\frac{dT_c}{dP}$decreasing with increasing doping [16]. Since T_c increases with increasing hole concentration to an optimum value, pressure induces changes in the bond lengths which intern can modify the electronic structure. This modification is rather small but it can result in a significant change in the hole carrier density in the two dimensional CuO_2 planes [35], [26].

In the $Y_1Ba_2Cu_3O_{7+\delta}$ family of superconductors, one can distinguish between two different pressure effects ($\frac{dT_c}{dP}$). There is the intrinsic pressure effect $(\frac{dT_c}{dP})_i$ which depends strongly on the oxygen content and shows a distinct maximum of 7.4K/GPa at $x = 6.72$. At this value of oxygen content, transition take place from the well defined 60 K plateau to the well defined 90 K plateau [31]. The other pressure effect $(\frac{dT_c}{dP})_o$ which induces oxygen ordering within the chains also shows a maximum at $x = 6.72$. For oxygen content close to 7, the pressure induced by oxygen ordering and the intrinsic pressure effects is zero or almost zero [35], [31].

At low temperatures close to T_c the ordering pressure effect is turned off which

enables researchers to determine the intrinsic pressure effect [31].

2.2 Residual Stress

High-T_c cuprates are promising superconducting materials in term of their possible applications. Optimization of the mechanical and superconducting properties of these materials continue to challenge physicists, engineers and material scientists. Elastic properties of $Y_1Ba_2Cu_3O_{7+\delta}$ depends strongly on its oxygen content. Furthermore, the elastic and mechanical properties of YBCO materials such as elastic moduli and stiffness are affected by the microstructural characteristics and defects inherent when producing these materials. The microstructure may reveal; porosity, line defects such as grain boundaries, twins, stacking faults and dislocations; point defects such as oxygen vacancies and interstitials; and structural order disorder, for example.

Elastic deformation of a polycrystalline piece of material is attained if the resulting strain is uniformly distributed over relatively large distances and lattice plane spacing change from their original stress free values to new stressed values. This long range stress is termed **macroscopic** stress or macrostress and gives rise to a **peak shift** in an x-ray diffraction pattern, for example. However, if the material is deformed plastically, lattice planes become distorted so that spacing of a particular (hkl) set of planes vary **from one grain to another** or may even varies **within the grains.** This short range stress is termed microscopic stress or microstress and gives rise to both a **peak shift** and **peak broadening** in the diffraction pattern [8], [19].

Before going any further into the subject of **residual stress,** it is important to

distinguish between applied stress and residual stress. Applied stress which is the force per unit area can be removed by removing the external force and the material will regain its stress free condition. Nonetheless, residual stress may develop by performing certain operations (deformation, substitutions, heating etc.) which will leave the material in a stressed condition even if all external forces have been removed. Residual stress, is thus, the stress that persists in the absence of an external forces or those stresses that are internally originated and contained in a material which has no external traction [8], [19].

As a consequence there are two kind of residual stresses in solids. There is macroresidual stress which may develop from mechanical processes such as surface working forming and assembly, thermal processes chemical processes. The second kind is the microresidual stress which extends over grains or within grains. This may originate from the anisotropic properties between grains or by difference in the mechanical properties of different, phases or regions in a material. It may also arise from defects such as dislocation pileups, kink boundaries and other microstructural phenomena. However, bulk values and hence macro-residual stresses are the most significant in fatigue and crack propagation and structural stability [8].

As mentioned above residual stress may develop from heat treatments which are critical in the synthesis of high T_c superconductors. In the preparation of $Y_1Ba_2Cu_3O_{7+\delta}$ material one has to anneal and quench the sample at high temperatures [48], [41]. This study will be concerned with measuring macroresidual stress.

2.2.1 Measurements and Formalism

Essentially, the strain in these HTSC materials needs to be measured in order to determine the stress by standard calculation method. Typically this requires the knowledge of the elastic constants of the HTSC materials and a calibration procedure. The residual stress is usually measured either by mechanical relaxation, which is a very slow destructive method, or by x-ray diffraction, a relatively fast non- destructive method. However, it is used to measure surface or near surface stress [48], [41].

Two techniques are commonly used in x-ray analysis of stress: line (width) profile analysis and measurements of the shift in d- spacing. Line (width) profile analysis is more involved and requires many standard samples for comparison. The d-spacing shift analysis is more direct and easy to perform. It is referred to as $\sin^2\psi$ analysis and it is a practical way in which to measure stress but it has some limitations. The diffraction pattern of the sample is performed as $\theta - 2\theta$ scan at different inclination of angles ψ. Different inclination angles causes some peaks to disappear from diffraction pattern owing to preferred orientation. The accuracy of this method increases when the analyzed peaks are selected at $2\theta > 2\psi_{\max}$ (two theta angles greater than twice the largest inclination angle). The surface stress is measured to a depth of about 20 microns which is the approximate average penetration depth of the x-ray beam [8].

2.2.2 Statement of the Problem

Changing the oxygen content affects the stress in the HTSC which leads to changes in the lattice spacing of various planes from their stress free values. This shift in lattice

spacing is essentially constant for a particular set of planes oriented similarly with respect to the stress. Thus, the shift in d-spacing (distances between crystal planes) is in principle a measure of stress [8], [19].

2.2.3 Theoretical Analysis

There are three principle stress components present within the stressed material; σ_1, σ_2 and σ_3, forming the so called biaxial or triaxial stress systems. If a surface of a polycrystalline material is stressed, then σ_1 and σ_2 are parallel to the surface and σ_3 is always zero at the surface. One can only measure two components of stress which lie in the plane of the surface. The general surface stress and the general strain is denoted by σ_φ and $\epsilon_{\varphi,\psi}$ on sequence. The term ψ is the angle between the surface normal and the direction of strain being measured [8]. By applying elasticity theory, we get the

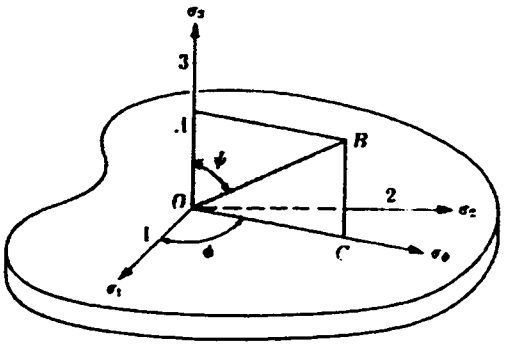

Figure 2.1: *Stresses at the surface of stressed body and the angles ψ, φ and the normal.*

following relationship which relates the measured strain to principal stresses [19]:

$$\epsilon_{\varphi,\psi} = \frac{1+v}{E}\left(\sigma_1 \cos^2\varphi + \sigma_2 \sin^2\varphi\right)\sin^2\varphi - \frac{\nu}{E}\left(\sigma_1 + \sigma_2\right) = \frac{d_{\varphi,\psi} - d_0}{d_0} \qquad (2.1)$$

where E is the Young modulus and v is the Poisson ratio for the material. In this equation, $d_{\varphi,\psi}$ is the spacing in the direction defined by φ and ψ and d_0 is the stress-free interplanar spacing. As we can see from the above equation, the strain ε_z normal to the surface is not zero, and is given by

$$\varepsilon_z = \epsilon_{\varphi,\psi=0} = -v(\epsilon_1 + \epsilon_2) = -\frac{v}{E}(\sigma_1 + \sigma_2) = \frac{d_{\varphi,\psi=0} - d_0}{d_0} \tag{2.2}$$

Also,

$$\sigma_\varphi = \sigma_1 \cos^2\varphi + \sigma_2 \sin^2\varphi \tag{2.3}$$

substituting equations 2.2 and 2.3 in 2.1 we get

$$\frac{1+v}{E}\sigma_\varphi \ \sin^2\psi = \frac{d_{\varphi,\psi} - d_{\varphi,\psi=0}}{d_0} \cong \frac{d_{\varphi,\psi} - d_{\varphi,\psi=0}}{d_{\varphi,\psi=0}} \tag{2.4}$$

Here we have replaced d_0 by $d_{\varphi,\psi=0}$ in the denominator. This approximation combined with the equation 2.4 is the heart of the x ray stress analysis method [19]. The approximation eliminates the need to know the unstressed plane spacing d_0. The stressed specimen needs to be examined at different ψ. The difference between two strains in the stressed sample depends only on the biaxial stress σ_φ acting in the plane, i.e.

$$\frac{d_{\varphi,\psi} - d_{\varphi,\psi=0}}{d_{\varphi,\psi=0}} = \frac{1+v}{E}\sigma_\varphi \ \sin^2\psi \tag{2.5}$$

where $d_{\varphi,\psi}$ is the d-spacing at inclination angle ψ and $d_{\varphi,\psi=0}$ is the d-spacing at the symmetric geometry ($\psi = 0$) [19], [41].

Chapter 3

Experimental Technique

3.1 Oxygen Stoichiometry

3.1.1 Sample Preparation

A key feature of copper oxides superconductors is that their superconducting properties are very sensitive to the method of synthesizing and annealing. Special attention has to be paid to preparation conditions; mixing, grinding, the calcination temperature and the sintering procedure to get a high quality homogeneous single phase sample [34], [1].

In general, there are three preparation methods for the HTSC's, namely, solid state, co-precipitation and the sol gel. In this thesis we only adhere to the first method which is the solid state reaction technique [54].

In the this method we start with an ultra pure powder (99.999%)of Y_2O_3, $BaCO_3$ and CuO. Materials were repeatedly ground and mixed for about an hour using a

mortar and pestle. During mixing and grinding a small amount of alcohol is added to the mixture to assure homogeneity of the mixture. The mixture was then placed in an alumina crucible and calcined in a furnace in air at 800°C for about 8 hours. After they are fast cooled overnight the samples are then re-ground and mixed. This mixing, grinding and calcination process is repeated at 850°C for about 5 hours, 900°C for about 6 hours and 950°C for about 15 hours. The samples were then re-ground and pressed into pellets of 2-3 mm thick and 10-13 mm diameter at a pressure of 400 kg/cm^2. During sintering heat treatment which is the final process, the sample pellets were heated in a tube furnace for 20 hours at a temperature of 950°C. The samples were then slow cooled to 400°C (1°C per minute) and then furnace cooled to room temperature. A continuous flow of oxygen was used during sintering to facilitate the removal of impurities and to allow oxygen uptake during the cooling stage. These annealed pellets were designated fully oxygenated (as prepared) $Y_1Ba_2Cu_3O_x$ polycrystalline samples.

3.1.2 Quenching Station

A fraction of the as prepared samples were annealed in nitrogen at 950°C and then slowly cooled to room temperature. These oxygen deficient and fully oxygenated (as prepared) samples (table 3.1) were used to produce samples with different oxygen contents by annealing at 600°c in nitrogen (to reduce their oxygen content) or in oxygen (to increase their oxygen content) gas flow for different annealing times. After reaching the annealing temperatures and times, samples were quenched into liquid

polycrystalline sample	wieght(mg)	volume(mm^3)
as prepared sample	102.7	$5.8 \times 3.37 \times 1.25$
oxygen deficient sample	100.6	$6.22 \times 3.54 \times 0.93$

Table 3.1: Sample dimensions

nitrogen using a quenching station. Quenching preserves the high temperature Physical state of the material. Samples were *fast quenched* into liquid nitrogen at 30 psi pressure.

The quenching station as it is shown in Fig. 3.1, consists of:

1. Tube furnace.

2. Quartz tube.

3. Nitrogen and oxygen gas cylinders.

4. Temperature controller.

5. Valves

Heat treatments and quenching conditions for all samples used in this thesis are presented in table 3.2. Also shown in table 3.3 are the changes in weight for selected samples. Table 3.4 list the oxygen content and the transition temperatures for all samples used in this thesis.

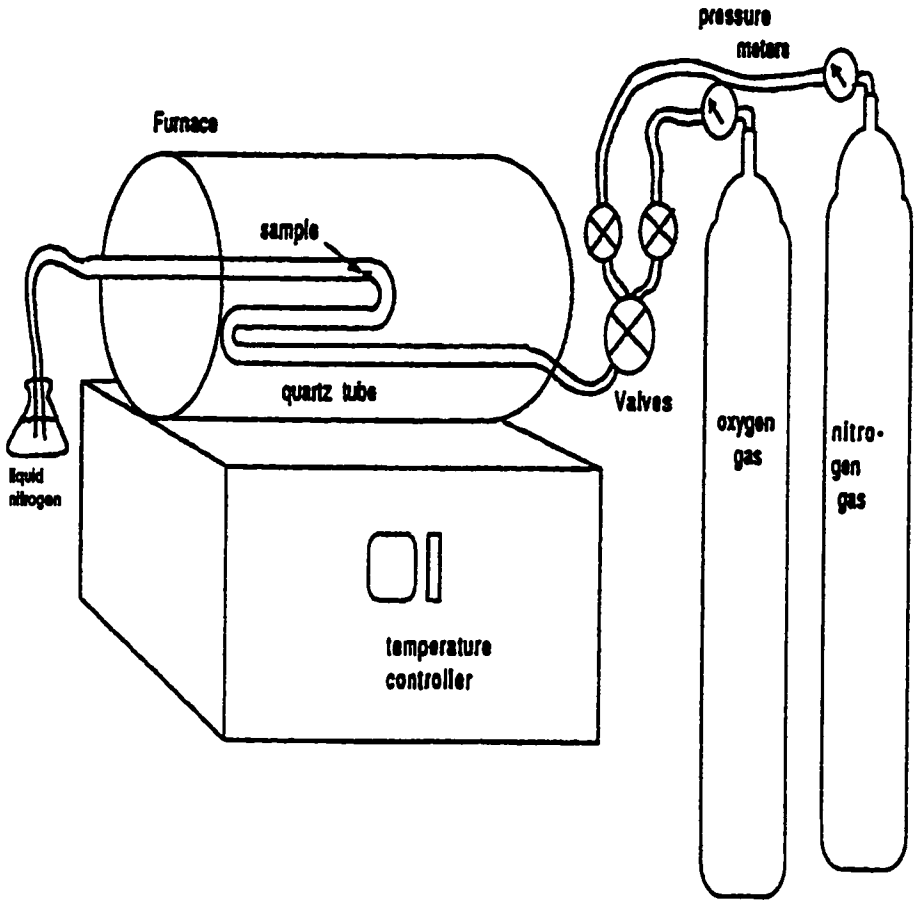

Figure 3.1: The quenching station designed and built in the superconductivty lab in the physics department which was used to produce different oxygen content samples.

Table 3.2: Heat treatment conditions for superconductor samples

Sample	Annealing time	Annealing temp.	Quenched to
as prepared	22h in O_2	950°C and then 550°C	room temp.
oxygen deficient	13h in N_2	950°C and then 550°C	room trmp.
YN_2Q_1	25m in N_2	600°C	LN_2
YN_2Q_2	12h in N_2	600°C	LN_2
YN_2Q_3	20m in N_2	600°C	LN_2
YN_2Q_4	10m in N_2	600°C	LN_2
YN_2Q_5	5m in N_2	600°C	LN_2
YO_2Q_6	12h in O_2	600°C	LN_2
YO_2Q_7	10h in O_2	900°C	LN_2
YO_2Q_8	20h in O_2	400°C	LN_2
YO_2Q_9	20h in O_2	250°C	LN_2
2qq	12h in N_2	600°C	LN_2

Table 3.3: Weight loss measurements of superconductor samples

SAMPLE	**WEIGHT LOSS**
YN_2Q_4	0.0048
YN_2Q_5	0.002
YO_2Q_6	-0.0004

Table 3.4: Oxygen content and Tc measurements

#	Sample	oxygen content	T_c (K)
1	as prepared	6.8382	90.2
2	oxygen deficient	6.7287	72.3
3	YN_2Q_1	6.4733	45.6
4	YN_2Q_2	6.3810	12.6
5	YN_2Q_3	6.5053	53.1
6	YN_2Q_4	6.8068	85.6
7	YN_2Q_5	6.7812	82.9
8	YO_2Q_6	6.8752	90.9
9	YO_2Q_7	6.3217	0.0
10	YO_2Q_8	6.9613	91.7
11	YO_2Q_9	6.9984	91.9
12	2qq	6.5167	64.0

3.2 Magnetization Measurements

Magnetization measurements were performed using a computer controlled Lakeshore-PAR (Princeton Applied Research) 9-Tesla vibrating sample magnetometer (VSM) (Model 4500/150A). This system is a combination of a VSM with a superconducting magnet which generates a high field up to 9 tesla and a variable temperature cryostat which ranges from less than 2 K up to 300 K. For detailed description of the system used refer to reference [10].

3.3 Characterization

3.3.1 Superconducting Properties

Superconductivity can be defined by two main properties namely: zero resistivity and magnetic field expulsion (Meissner effect) hence two routes are usually used to characterize the samples ; magnetization measurements and resistivity measurements. The former which we used gives a good experimental indicator of the overall superconducting state while the latter is good for practical purposes. A sharp transition temperature measured by either method is a good indicator of high a quality sample.

To characterize the HTSC samples magnetization measurements were employed to measure the transition temperature by monitoring the magnetization response as the temperature increases in the presence of low magnetic field. We also used the varations in the c-axis as a measure of the transition temperature (see chapter 4).

3.3.2 Structural Analysis

In addition to the investigation of superconducting properties one needs to inspect the structural properties of the sample. This can be done by X-ray powder diffraction (XRD) or neutron powder diffraction. The XRD technique was used and the diffraction peaks were measured for each 2θ angle which is related to the d-spacing in the structure of the sample. Phase identification was performed and the lattice parameters were determined from the diffraction peaks at zero inclination angle ($\psi = 0$) and varying $\theta - 2\theta$ pattern.

XRD patterns of the pellet samples were obtained using a computer controlled PHILIPS PW1710 diffractometer at the King Fahd University of Petroleum and Minerals Research Institute. The XRD was equipped with Cu-Kα radiation of wave length (average $\lambda = 1.541838$ Å) with a Cu broad focus tube energized to 45 kv and 30 mA. The angle 2θ was scanned over the range from 5 to 80 degrees. The lattice parameters calculations and indexing were done on powder diffraction package (PDP) software.

3.4 Stress Measurements

As mentioned in chapter 2, if the surface is stressed, due to Poisson effect, the planes are further apart than in the stress-free state. This shift in lattice spacing is essentially constant for a particular set of planes oriented similarly with respect to the stress. Thus, the shift in d-spacing (distances between crystal planes) is in principle a measure of stress see Fig. (3.2).

For the stress measurements a PHILIPS PW1710 diffractometer was used. After

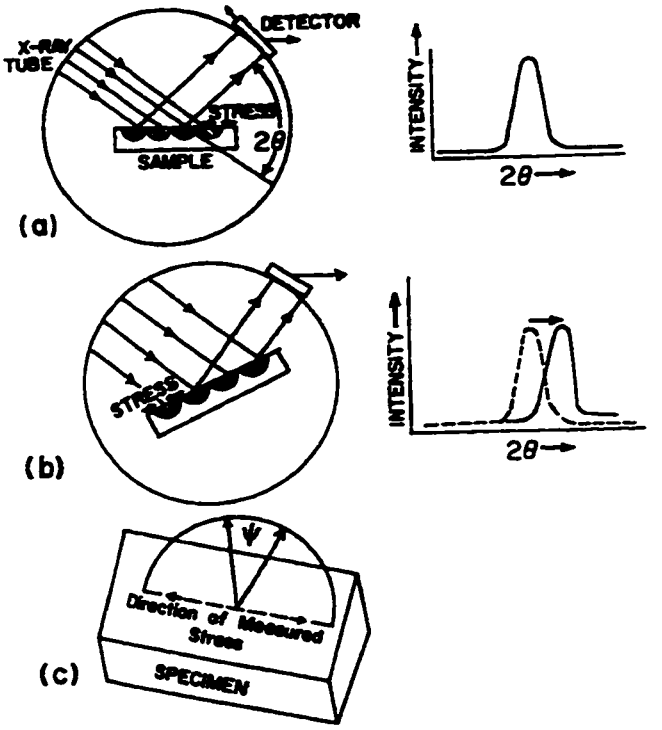

Figure 3.2: *The use of a diffractometer for stress measurement at various inclination angles ψ.*

a diffraction pattern was obtained for the zero inclination angle for all samples (as prepared sample, oxygen deficient sample and quenched samples), the sample is then tilted to a given ψ-angle in a direction perpendicular to the plane in which $\theta - 2\theta$ varies. Diffraction patterns were produced at different inclination angles ψ $(10, 20, 30)$. Several values of lattice strains$\left(\frac{d_{\varphi,\psi} - d_{\varphi,\psi=0}}{d_{\varphi,\psi=0}}\right)$ are measured each at different angles ψ $(10, 20, 30)$.

Chapter 4

Results and Discussion

4.1 Crystal structure

The crystal structure characterization and analysis of all samples were done by the x-ray diffraction technique. Diffraction patterns were obtained for all samples used in this study. Fig. 4.1 and 4.2 show the XRD pattern for the two types of samples that we have used to produce samples with different oxygen contents.

The XRD pattern for the as prepared fully oxygenated sample is shown in Fig. 4.1. The structure is orthorhombic with lattice parameters and unit cell volume shown in table 4.1. These numbers are in agreement with published data, namely $\mathbf{a} = 3.823$, $\mathbf{b} = 3.887$, $\mathbf{c} = 11.680$ [20]. The sample is a superconductor with $T_c = 90.2$ K.

The the oxygen deficient (partially deoxygenated) sample XRD pattern is shown in Fig. 4.2. These sample is produced by annealing the fully oxygenated samples in nitrogen flow for a long time (see chapter 3). Though this procedure reduced the oxygen content of the sample, it does not transform it into a tetragonal structure.

Table 4.1: Structural parameters of YBCO with varying oxygen content

Sample	c(Å)	x-value	T_c(K)	a(Å)	b(Å)	abc(Å^3)	δ	$\frac{b-a}{b+a} \times 1000$
YO_2Q_7	11.779	6.322	0.0	3.857	3.857	175.209	0.678	0.000
YN_2Q_2	11.768	6.381	12.6	3.868	3.868	176.090	0.619	0.000
YN_2Q_1	11.752	6.473	45.6	3.860	3.860	175.103	0.527	0.000
YN_2Q_3	11.747	6.505	53.1	3.871	3.871	176.037	0.495	0.000
2qq	11.745	6.517	64	3.870	3.870	175.925	0.483	0.000
oxygen deficient	11.707	6.729	72.3	3.816	3.884	173.501	0.271	8.884
YN_2Q_5	11.698	6.781	82.9	3.832	3.881	173.980	0.219	5.340
YN_2Q_4	11.694	6.807	85.6	3.816	3.880	173.124	0.193	8.277
as prepared	11.688	6.838	90.2	3.821	3.885	173.502	0.162	8.240
YO_2Q_6	11.682	6.875	90.9	3.827	3.883	173.575	0.125	7.186
YO_2Q_8	11.667	6.961	91.7	3.815	3.885	172.910	0.039	9.000
YO_2Q_9	11.660	6.998	91.9	3.820	3.870	172.412	0.002	6.501

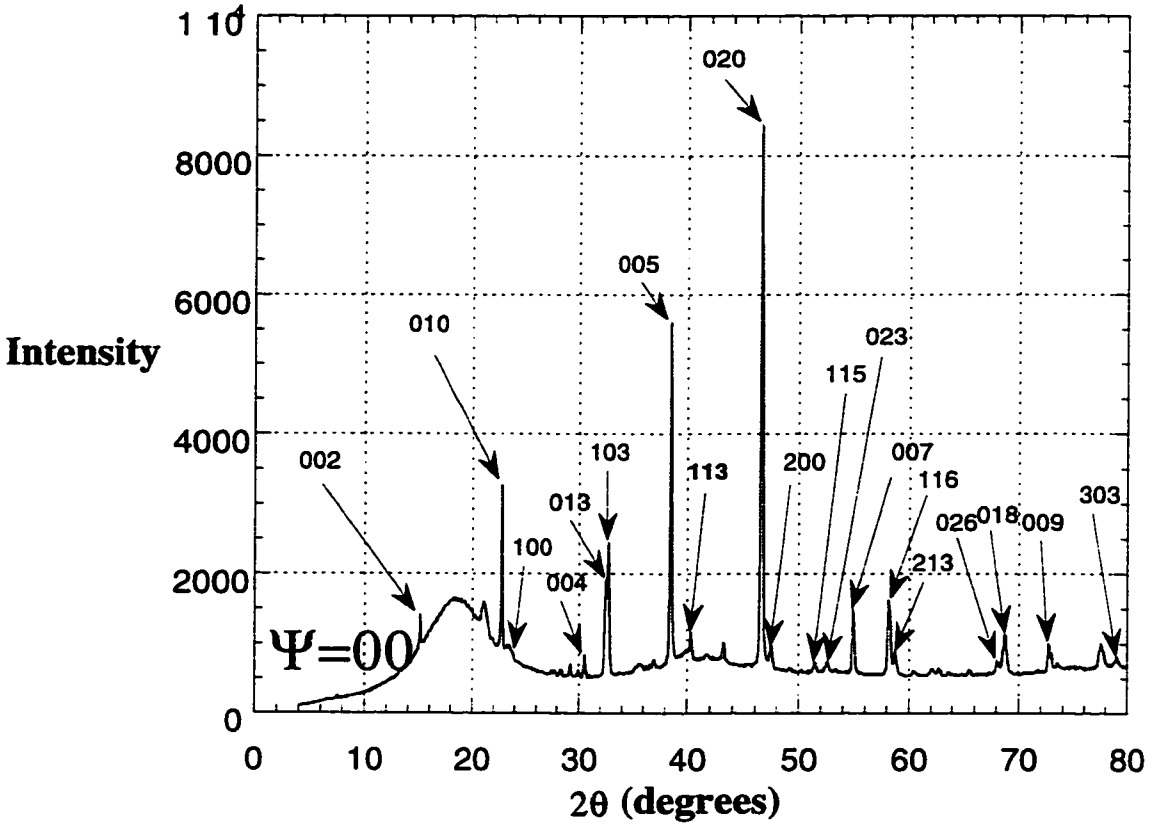

Figure 4.1: *X-ray diffraction pattern of as prepared YBCO sample at* $\psi = 0$.

The XRD pattern for the de-oxygenated sample is shown in Fig.A.3 which corresponds to the first sample in table 4.1. The structure is tetragonal and the lattice parameters are also listed in table 4.1. The sample is non-superconducting.

XRD patterns for all samples with varying oxygen content were first indexed and refined (at zero tilt angle $\psi = 0$) to obtain the lattice parameters for each sample. This was done using the PDP version 1.1 software on a 60386 personal computer.

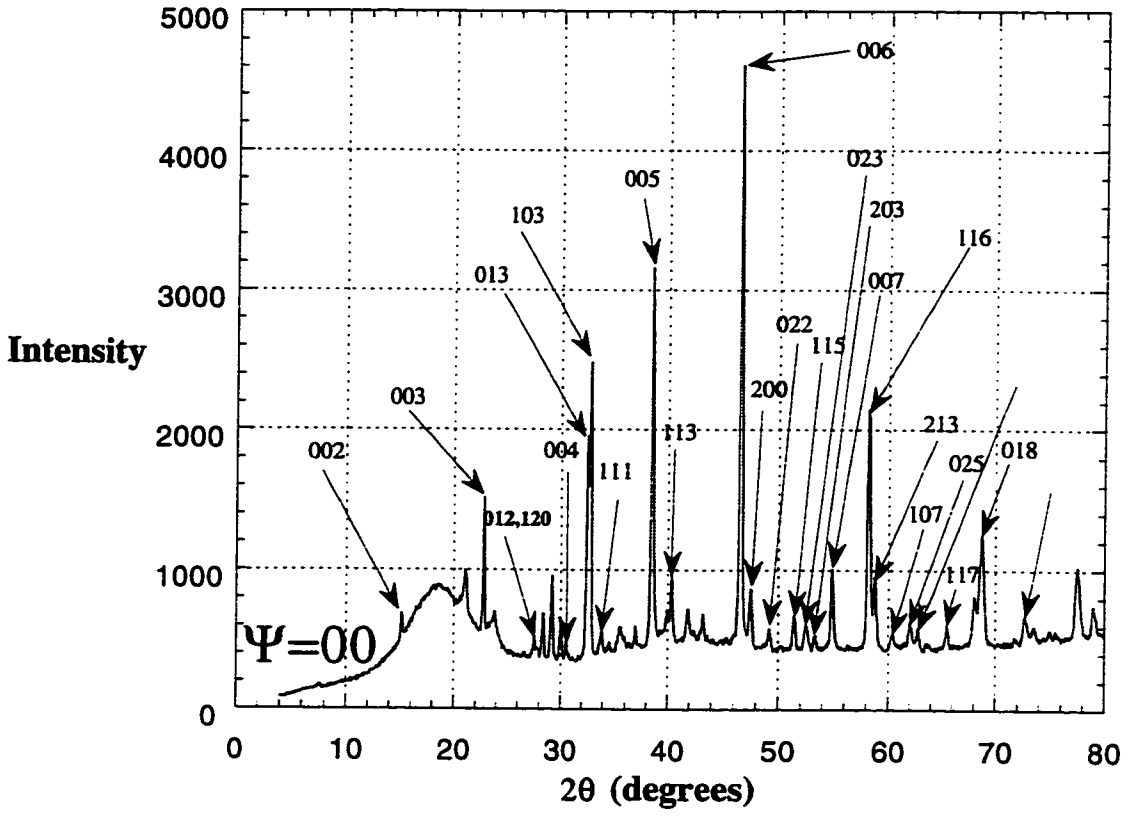

Figure 4.2: *X-ray diffraction pattern of oxygen deficient YBCO sample at* $\psi = 0$.

The resulting lattice parameters were obtained and they are tabulated in table 4.1. Results of the calculated structures were generally in agreement with published data for YBCO tetragonal and orthorhombic phases [20], [25], [28], [46], [21].

The difference in intensities of some peaks is due to texture or preferred orientation since the diffraction patterns were produced from samples in a pellet form rather than powder form. This leads to preferred orientation along the c-axis since YBCO is highly

anisotropic.

4.2 Variation of Lattice Parameters with Oxygen Content

The variations of the lattice parameters (**a**, **b** and **c**) with oxygen content in YBCO material were extensively investigated by many groups [20], [25], [28], [46]. It was shown that the values of these parameters are affected by the oxygen content in the YBCO as well as other materials.

4.2.1 Variation of c-axis

The variation of the **c**- axis with oxygen content have been found to decrease linearly as the oxygen content increases [20], [25]. Literature data by independent groups obtained by iodometric titration, x-ray diffraction analysis and oxygen weight loss [20], [28], [46] were used to fit a linear relationship relating the oxygen content and c-axis length and this is plotted in Fig. 4.3. We have compiled the **c**-axis and the oxygen content data obtained by Vanderah et al. [28], Parks et al. [46] and Jorgensen et al. [20] and used the linear fit to obtain the following:

$$x = 73.47 - 5.701c \tag{4.1}$$

with reliability of fit = 0.98 were x is the oxygen content and c is the lattice parameter of the c-axis.

The relation 4.1 was used later to obtain the oxygen content for each sample used

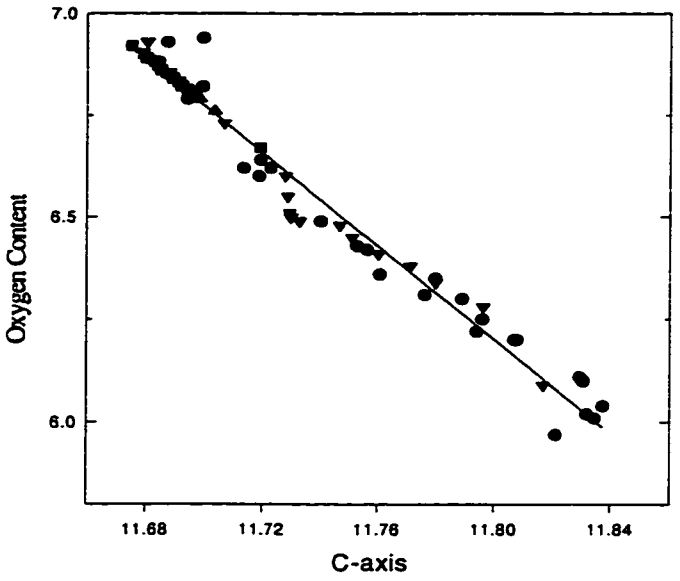

Figure 4.3: *Oxygen content versus c-axis lattice prameters in YBCO[20],[28],[46].*

in this thesis after obtaining the refined value of the c-axis using data from the XRD pattern for each sample. The results are shown in table 4.1.

4.2.2 Variation of the a,b axis

The x values obtained using eqn. 4.1 were used along with **a** and **b** parameters obtained from XRD pattern to generate the variations of **a** and **b** with oxygen content presented in Fig. 4.4. The **a,b** parameter values obtained from the refinement of the x-ray patterns of all were in good agreement with the literature data [20], [25], [46].

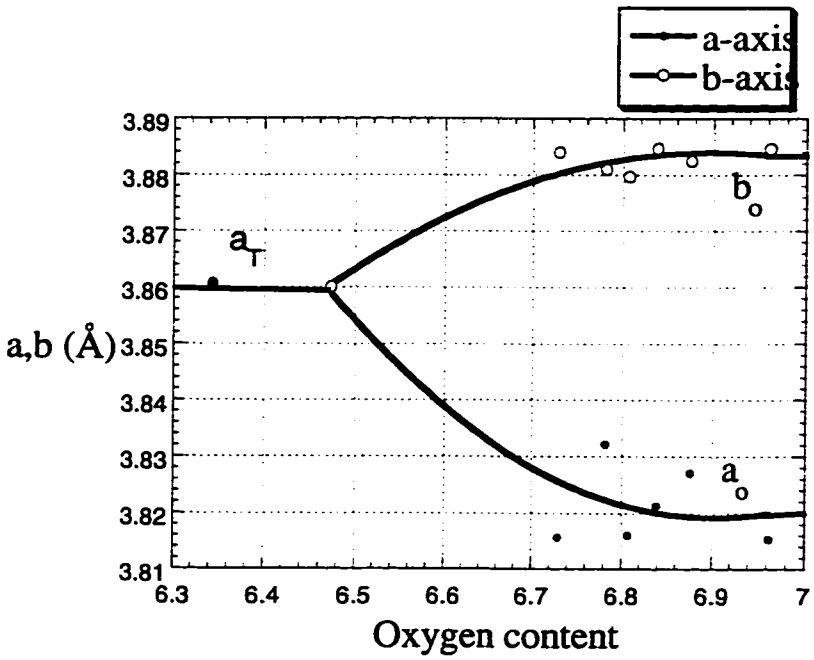

Figure 4.4: *Lattice parameters a and b versus oxygen content in YBCO.*

4.2.3 Variation of the Lattice Volume

The combined effects of oxygen content on the variations of the lattice parameters can be seen through the volume changes. The orthorhombic and tetragonal volume of the unit cell is given as $\mathbf{V = abc}$. The data shown in Fig. 4.3 and Fig. 4.4 are used to generate Fig. 4.5 and Fig. 4.6. Linear fit is used to obtain the following:

$$V = 172.62 + 5.21\delta \tag{4.2}$$

The first term in the above eqn. V_0 is the volume of the unit cell at $\delta = 0$ or oxygen content $x = 7$ which correspond to fully oxygenated orthorhombic unit cell.

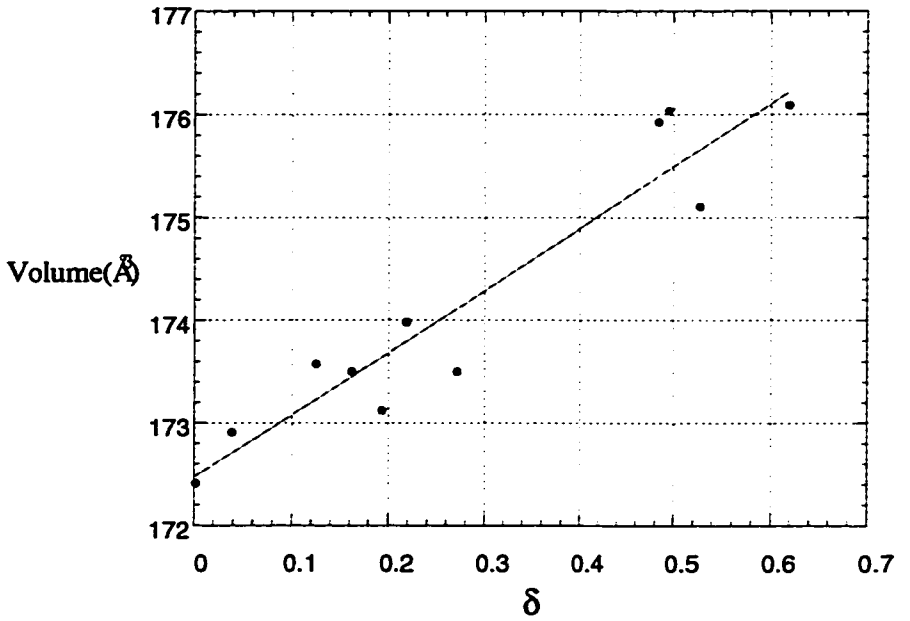

Figure 4.5: *Cell volume versus δ in YBCO. It is apparent that as oxygen is removed the volume increases.*

4.2.4 Variation of Orthorhombicity

Orthorhombicity $\left(\frac{b-a}{b+a} \times 1000\right)$ as defined in the literature [43] is a measure of how much of the structure is orthorhombic. As Orthorhombicity decreases to zero, the Orthorhombic structure collapses into tetragonal symmetry. In YBCO material this is shown in Fig. 4.7 which can be explained as follows:

At oxygen stoichiometry = 7, all the available $O(1)$ sites that form the one dimensional chain along the **b** direction is occupied. The $O(5)$ sites along the **a** direction is empty. Consequently the **b** lattice constant is longer than **a** and the difference **(b – a)** is the highest. As oxygen is removed the occupancies of the $O(1)$ sites is

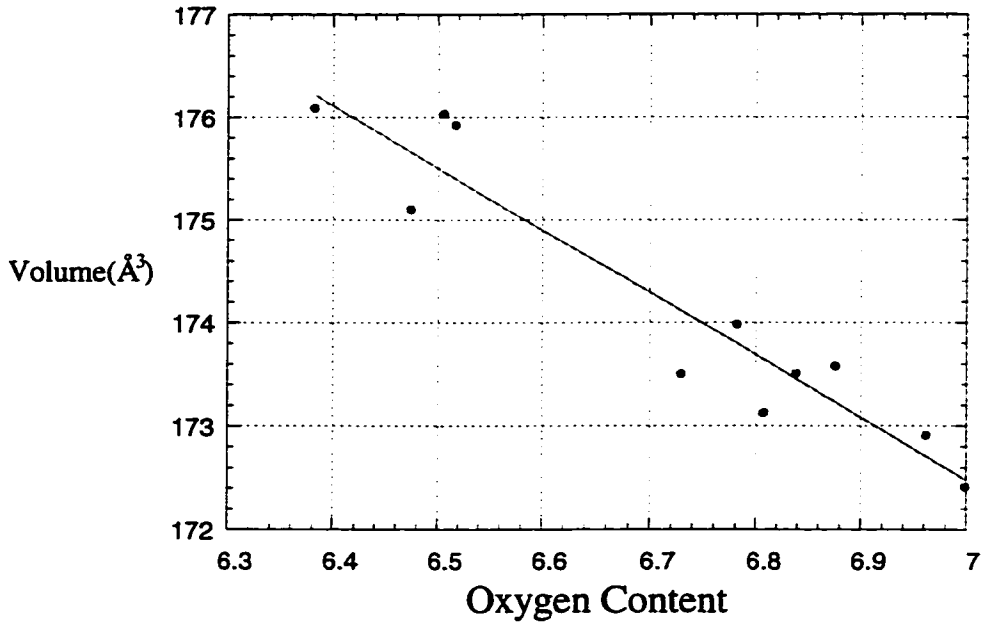

Figure 4.6: *Variation of volume of the unit cell with oxygen content. It is apparent that as oxygen is added the volume decreases.*

lowered so the difference (**b** − **a**) and occupancy of $O(5)$ sites is near zero. At $\delta < 0.5$ the occupancy of $O(5)$ sites rises rapidly to meet the occupancy of $O(1)$ sites at the orthorhombic to tetragonal phase transition and the value of **a** and **b** lattice constants are equal and the difference (**b** − **a**) is zero. Similar argument applies to the residual stress as we will discuss later in this chapter.

4.3 Magnetic Properties

Magnetic characterization of the sample was done by measuring the variation of the magnetization of the samples as a function of field while cycling the field between

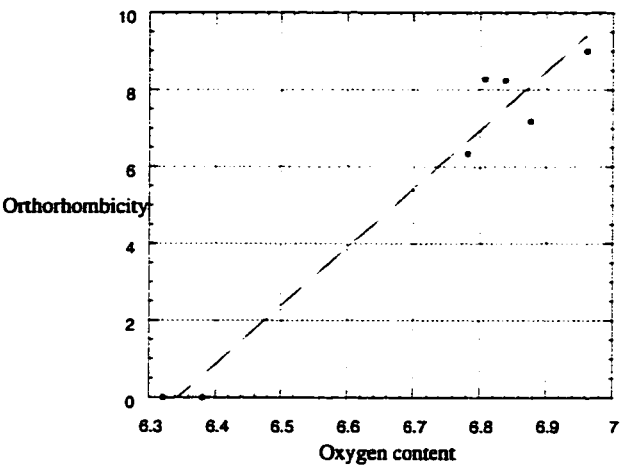

Figure 4.7: *Orthorhombicity* $\left(\frac{b-a}{b+a} \times 1000\right)$ *versus oxygen content in YBCO.*

± 9 T at a fixed temperature (4.2 K). Hysteresis loops were produced for all samples as seen in Figs 4.8 and 4.9. Samples with a tetragonal structure are those reported in Fig 4.8 with oxygen content less than 6.4 and they appear without any apparent hysteresis. This is an indication that the material is non-superconducting or there is no flux lattice structure. For the sample yo2q7 the variation of magnetization with field shows a small signal with no hysteresis indicating that for this particular oxygen content there is a very small portion of the sample in the superconducting state. Samples with an orthorhombic structure are shown in Fig 4.9 and they have hysteresis loops with different areas reflecting different annealing history.

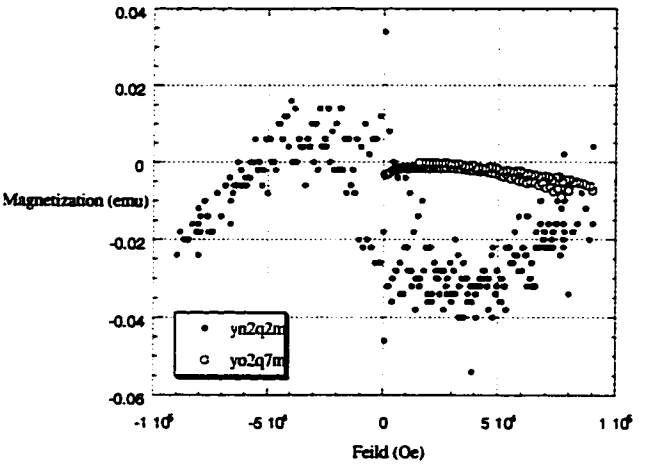

Figure 4.8: *Hysteresis loops for tetragonal YBCO sample produced by cycling the field between ±9 T at a fixed temperature (4.2 K).*

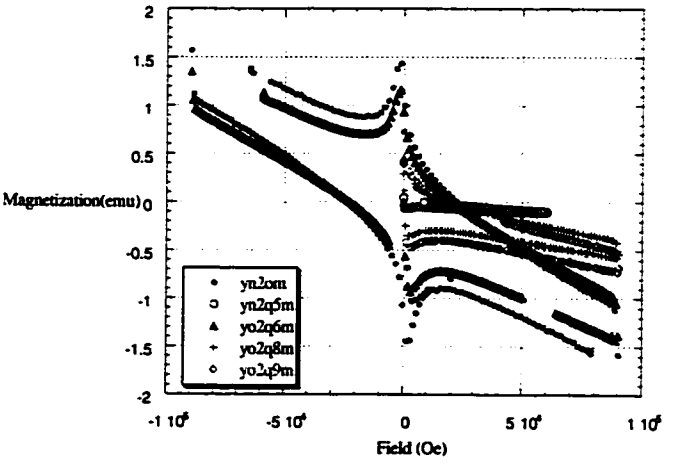

Figure 4.9: *Hysteresis loops for orthorhombic YBCO samples produced by cycling the field between ±9 T at a fixed temperature (4.2 K).*

4.4 X-ray Diffraction

For each of the samples used in this study four $(\theta - 2\theta)$ x-ray diffraction patterns were obtained. For $\psi = 0$ inclination angle, diffraction patterns were refined and consequently the lattice parameters **a**, **b** and **c** were obtained. The other three patterns for $\psi = 10$, 20, 30 inclination angle were used and combined with $\psi = 0$ inclination pattern to obtain the shift in d-spacing values caused by the residual stress (see chapter 2). The XRD pattern for non-quenched samples are shown in Fig. 4.10.

4.4.1 Strain Identification and the Application of $\sin^2\psi$ Method

The strain $\varepsilon = \frac{d_\psi - d_{\psi=0}}{d_{\psi=0}}$ was determined for observed planes in all samples. For each plane the strain is plotted against $\sin^2\psi$ and a best fit for a strait line as described by the equation below is drawn for each plane. Some of the results for selected planes are shown in Figs 4.11 and 4.12.

$$\frac{d_{\varphi,\psi} - d_{\varphi,\psi=0}}{d_{\varphi,\psi=0}} = \frac{1+\nu}{E}\sigma_\varphi \sin^2\psi \tag{4.3}$$

The residual stress is proportional to the slope of ε versus $\sin^2\psi$. Slopes of some of the planes corresponding to different samples with different oxygen content and annealing history appear in tables A.1 through A.5.

4.4.2 Phase Diagrams

Phase diagrams were reported in the literature to show the variation of transition temperature T_c with oxygen content (x) [14], [20], [25], [30] and [53] (see Figs 1.6 and 1.7 in chapter 1). This approach is now applied to the construction of phase diagrams for the variation of residual stress with oxygen content and T_c from the new research data in this study.

4.4.3 Variation of Stress with Oxygen Content

Slopes versus oxygen content were plotted for certain planes the (006) planes and the and mixed index planes to observe the behavior of the stress along the c-axis and in the ab-planes. The results are shown in Figs 4.13, 4.14. Within the accuracy of our measurement in the orthorhombic phase, the residual stress is seen to increase as the oxygen content is increased.

4.4.4 Variation of Stress with Transition Temperature

The phase diagram for the variation of stress with T_c is constructed. Results are shown in Figs 4.15, 4.16. Within the accuracy of our measurements, the residual stress increases as the oxygen content is increased with a rapid increase at 60K.

4.5 Discussion

It is relatively recent that attempts have been made to measure the residual stress in the HTSC,s [36], [48], [41]. However, extensive study on the effect of residual stress

have to be made to achieve more systematic understanding of growth mechanisms process technology, weak links, fracture mechanisms etc. For YBCO material, we tried to study the effect of variation of oxygen content on the residual stress. These measurements shows an increase in the residual stress (for (006) plane) with increasing oxygen content for the orthorhombic structure. As residual stress increases T_c also increases. This is understood in view of the structure of the YBCO material. The value of oxygen content x ranges from 6 to 7. At $x = 6$, both the $O(1)$ site and $O(5)$ are empty and **a** and **b** lattice constants are equal and the structure tetragonal. As the oxygen is added to the structure (x is increased), $O(1)$ site and $O(5)$ are equally occupied. At a critical value (x=6.48), a phase transformation occurs to form the orthorhombic structure with the $O(1)$ sites that form the one dimensional chain along the **b** direction become occupied and the $O(5)$ sites are left empty. The lattice constant along **b** increases and the lattice constant along **a** decreases. As a result, strain in the **ab** plane increases and hence the residual stress. This is combined with a smooth decrease in the lattice parameter along the **c** direction. It is common to all residual stresses that a tensile stress in one direction is balanced with a compressive stress in another.

Results obtained from the (006) reflection indicates that as the oxygen content changes, the slope increases (Fig. 4.13) and T_c also increases with x (Fig. 4.15). This is attributed to a compressional stress which results in a reduction of the **c**-axis. XRD reflections obtained from mixed (hkl) indicates little internal changes in the slope (Fig. 4.15) and in T_c (Fig. 4.16). This may be related to tensile stress in the ab plane. More results are presented in Appendix A.

Changes in T_c disordered material may be also related to the residual stress induced by disorder phenomena which is a subject that should be further studied.

The volume of the unit cell remarkably increases as the oxygen is removed as shown in Fig. 4.5 or equivalently decreases as oxygen is added as shown in Fig. 4.6. This is an unexpected result sense common since says that if oxygen is added the volume will increase. However, this is not the case because as oxygen was added it occupied certain energetically favorable sites. This is in qualitative consistency with previous work by Jorgensen et al. [20] and Cava et al. [25].

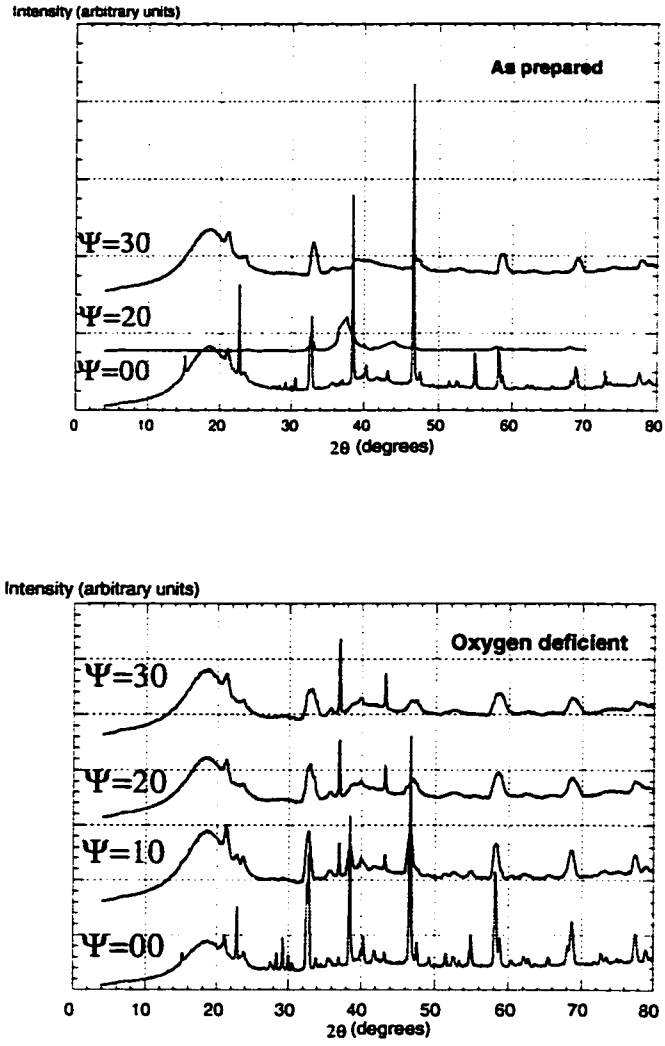

Figure 4.10: *X-ray diffraction patterns of YBCO as prepared (top) and oxygen deficient (bottom) for various angles* $\psi = 00, 10, 20, 30$.

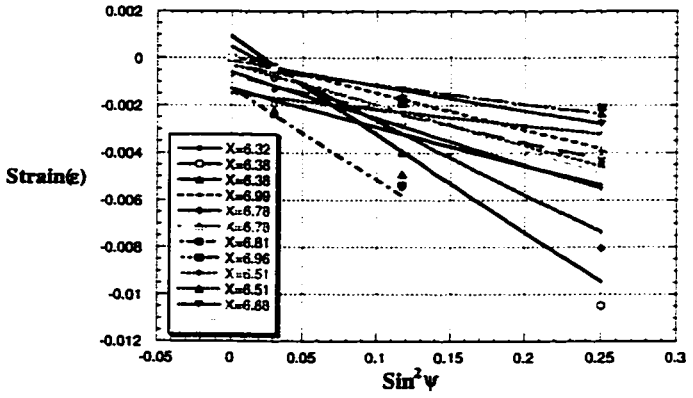

Figure 4.11: *Slopes (stresses) from strain versus* $\sin^2\psi$ *YBCO with varying oxygen content for the (115) planes.*

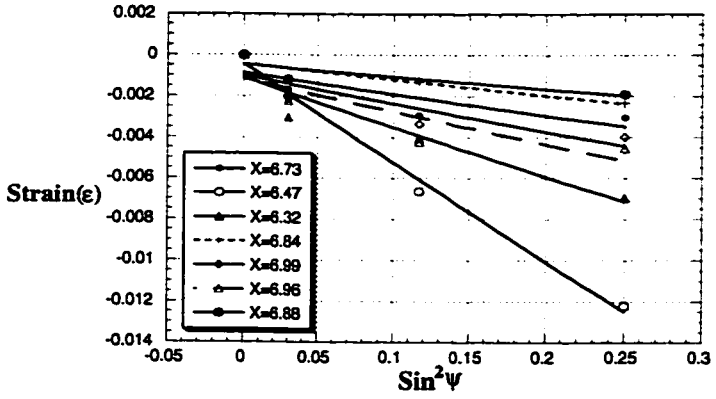

Figure 4.12: *Slopes (stresses) from strain versus* $\sin^2\psi$ *YBCO with varying oxygen content for the (006) planes.*

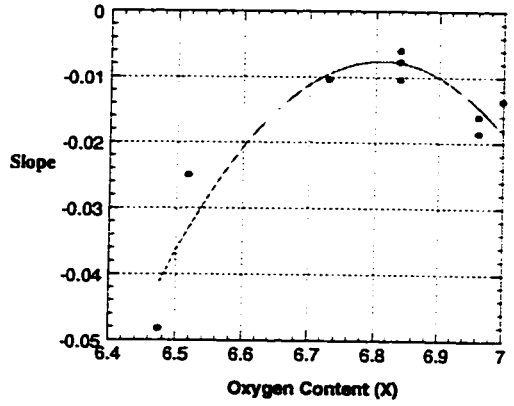

Figure 4.13: *Variation of slopes with oxygen content for (006) reflection. This shows that a compressional residual stress increases with increasing oxygen content.*

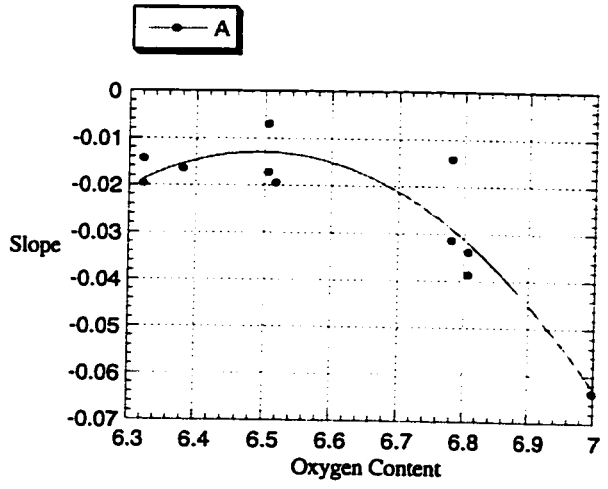

Figure 4.14: *Variation of slopes with oxygen content for (115) reflection. This shows that the overall tensile residual stress in the ab-plane increases with increasing oxygen content.*

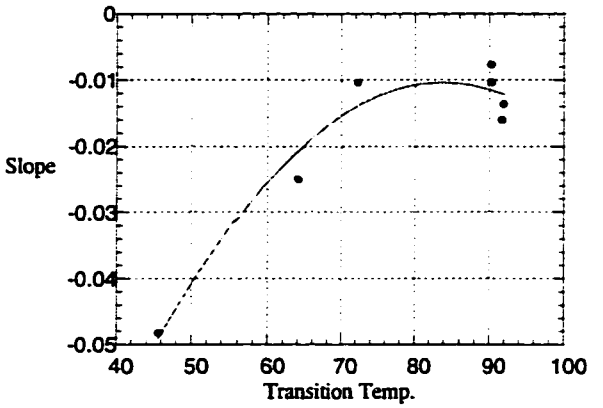

Figure 4.15: *Variation of slopes with transition temperature for (006) reflection. This shows that T_c increases by increasing compressional residual stress.*

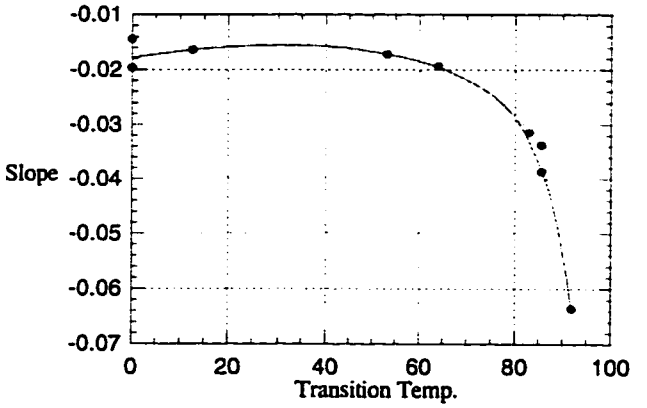

Figure 4.16: *Variation of slopes with transition temperature for (115) reflection. This shows that along the ab-plane the residual stress increases by increasing the overall tensile stress.*

Chapter 5

Conclusion

Samples of different oxygen content were prepared by annealing in O_2 and N_2 gases for different times at 600° C. After fixing the oxygen content, samples were FAST quenched using home made quenching station to freeze the high temperature state.

Different data from independent sources was used to plot the relation between c-axis parameter and the oxygen content and the transition temperature T_c. From this relation it is apparent that the measured c-axis parameter length varies linearly and is sensitive to the variation of the oxygen content and T_c in this study.

Relation between **a** and **b** parameters and the oxygen content were constructed which show a transition from orthorhombic to tetragonal at $x \sim 6.48$.

Orthorhombicity and volume of the unit cell were plotted against oxygen content and an unexpected volume contraction of the unit cell was observed. This can be explained by noting that as oxygen was added to the unit cell it can occupy certain sites which are energetically favorable.

X-ray diffraction patterns at different inclination angles were obtained and refined

for all samples and best fit for the relation between strain and the $\sin^2\psi$ were plotted.

Slopes of the strain versus $\sin^2\psi$ which is proportional to the residual stress were plotted against oxygen content for certain reflections (006) and (115).

Different behaviors for the two reflections (006) and (115) were noted which is attributed to compressional and tensile stresses. Along the c-axis compressional stress increases with increasing oxygen content whereas the overall tensile residual stress in the ab-plane increases with increasing oxygen content. Also T_c increases by increasing the compressional residual stress along the c-axis but in the ab-plane it increases by increasing the overall tensile stress.

This explains the relatively high hydrostatic pressure effect for oxygen deficient YBCO compared to a very small (nearly zero) effect for fully oxygenated material ($x = 7$). Since as the material reaches saturation for fully oxygenated sample no more oxygen can be added which in turn changes the residual (internal) stress. Also, this suggest that changes in T_c for disordered material is due to changes in the residual stress induced by disorder phenomena which is a subject that should be further studied.

Two shortcomings were encountered in using this technique. First, is the disappearance of XRD peaks at higher inclination angle due to preferred orientation. Second, separation of the residual stress in the ab-plane.

Improvement of this technique can be achieved by lowering the degree of preferred orientation by preparing grain oriented samples to separate the residual stress in the ab-plane and using additional smaller inclination angle (ψ). These improvements are under way in our lab.

Appendix A

Additional Results

A.1 Tables for Slopes and Oxygen Contents

Table A.1: Slopes (stress) for the (005) planes in YBCO

#	Sample	Slope	Reliability of fit	Oxygen Content
1	YN_2Q_1	-0.048274	0.992914	6.4733
2	2qq	-0.024997	0.370544	6.5167
3	YO_2Q_9	-0.013671	0.790689	6.9984

Table A.2: Slopes (stress) for the (116) planes in YBCO

#	Sample	Slope	Reliability of fit	Oxygen Content
1	YO_2Q_7	-0.019626	0.617197	6.3217
2	YN_2Q_5	-0.014157	0.866231	6.7812
3	YN_2Q_4	-0.038653	0.698069	6.8068
4	YO_2Q_6	-0.010706	0.992689	6.8752
5	YO_2Q_8	-0.08187	0.788116	6.9613
6	YO_2Q_9	-0.015720	0.994497	6.9984

Table A.3: Slopes (stress) for the (006) planes in YBCO

#	Sample	Slope	Reliability of fit	Oxygen Content
1	YO_2Q_7	-0.024227	0.995412	6.3217
2	oxygen deficient	-0.010369	0.679438	6.7287
3	as prepared	-0.007696	0.829065	6.8382
4	YO_2Q_6	-0.005973	0.724640	6.8752
5	YO_2Q_8	-0.016026	0.735773	6.9613
6	YO_2Q_9	-0.018545	0.820288	6.9984

Table A.4: Slopes (stress) for the (115) planes in YBCO

#	Sample	Slope	Reliability of fit	Oxygen Content
1	YO_2Q_7	-0.014380	0.995412	6.3217
2	YN_2Q_2	-0.041514	0.901429	6.3810
3	YN_2Q_3	-0.006980	0.227203	6.5053
4	2qq	-0.019436	0.989346	6.5167
5	YN_2Q_5	-0.031426	0.919197	6.7812
6	YN_2Q_4	-0.033771	0.936859	6.8068
7	YO_2Q_9	-0.063628	1.000000	6.9984

Table A.5: Slopes (stress) for the (117) planes in YBCO

#	Sample	Slope	Reliability of fit	Oxygen Content
1	YN_2Q_2	-0.016362	0.650620	6.3810
2	YN_2Q_3	-0.017185	0.954337	6.5053

A.2 Variation of T_c with Orthorhombicity

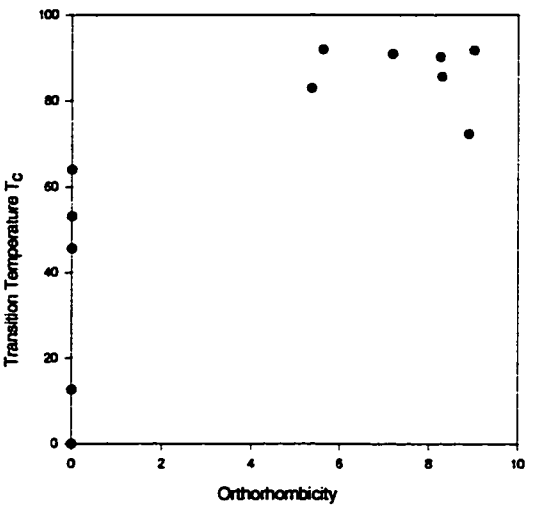

Figure A.1: *Variation of T_c with orthorhombicity in YBCO material.*

Variation of T_c with orthorhombicity is shown in Fig. A.1. It has been found that as oxygen content increases T_c increases to an optimum value.

A.3 XRD Patterns for Quenched Samples.

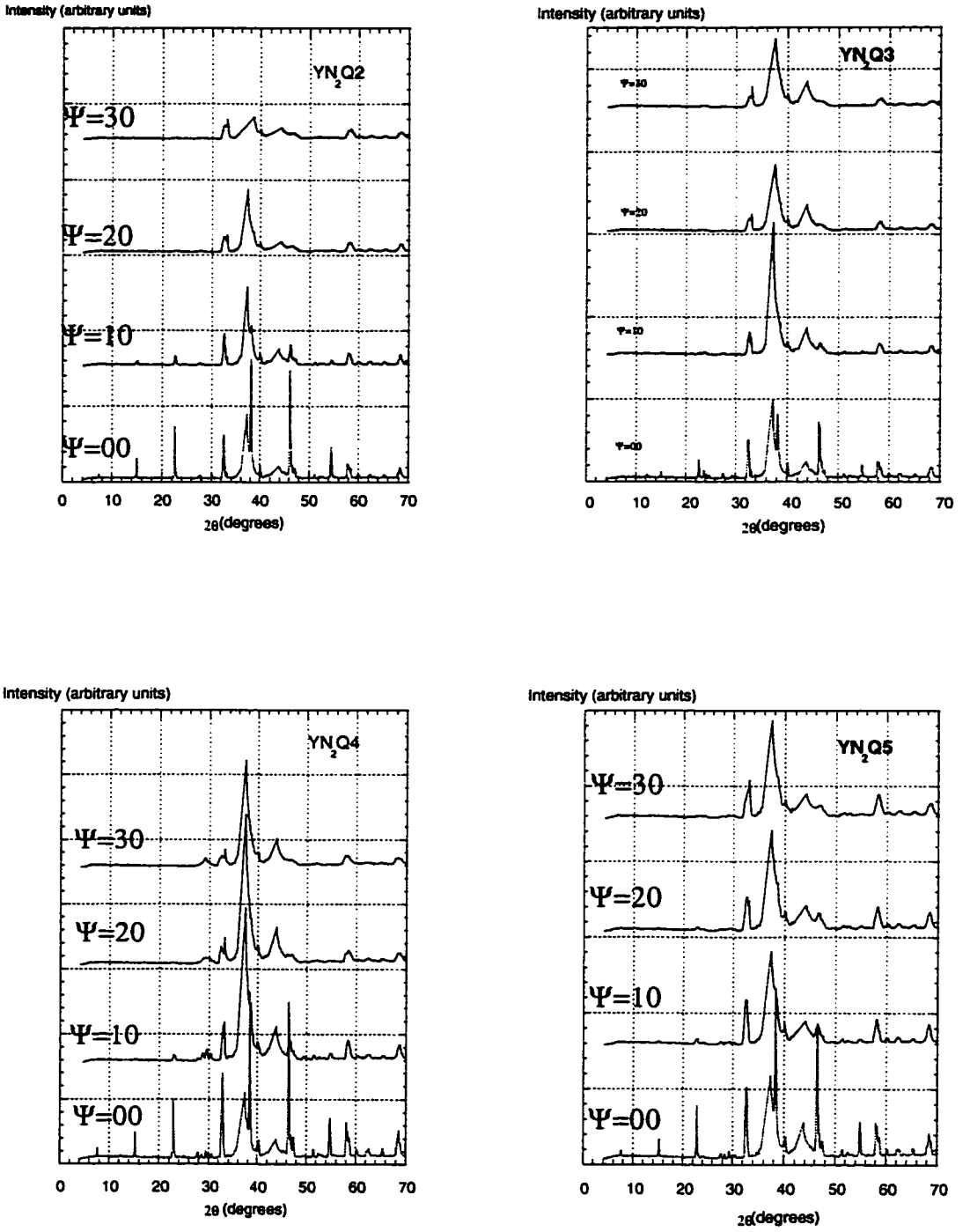

Figure A.2: *Different samples annealed in nitrogen gas for different time periods and then quenched to liquid nitrogen refer to table 3.2 for the history of each sample.*

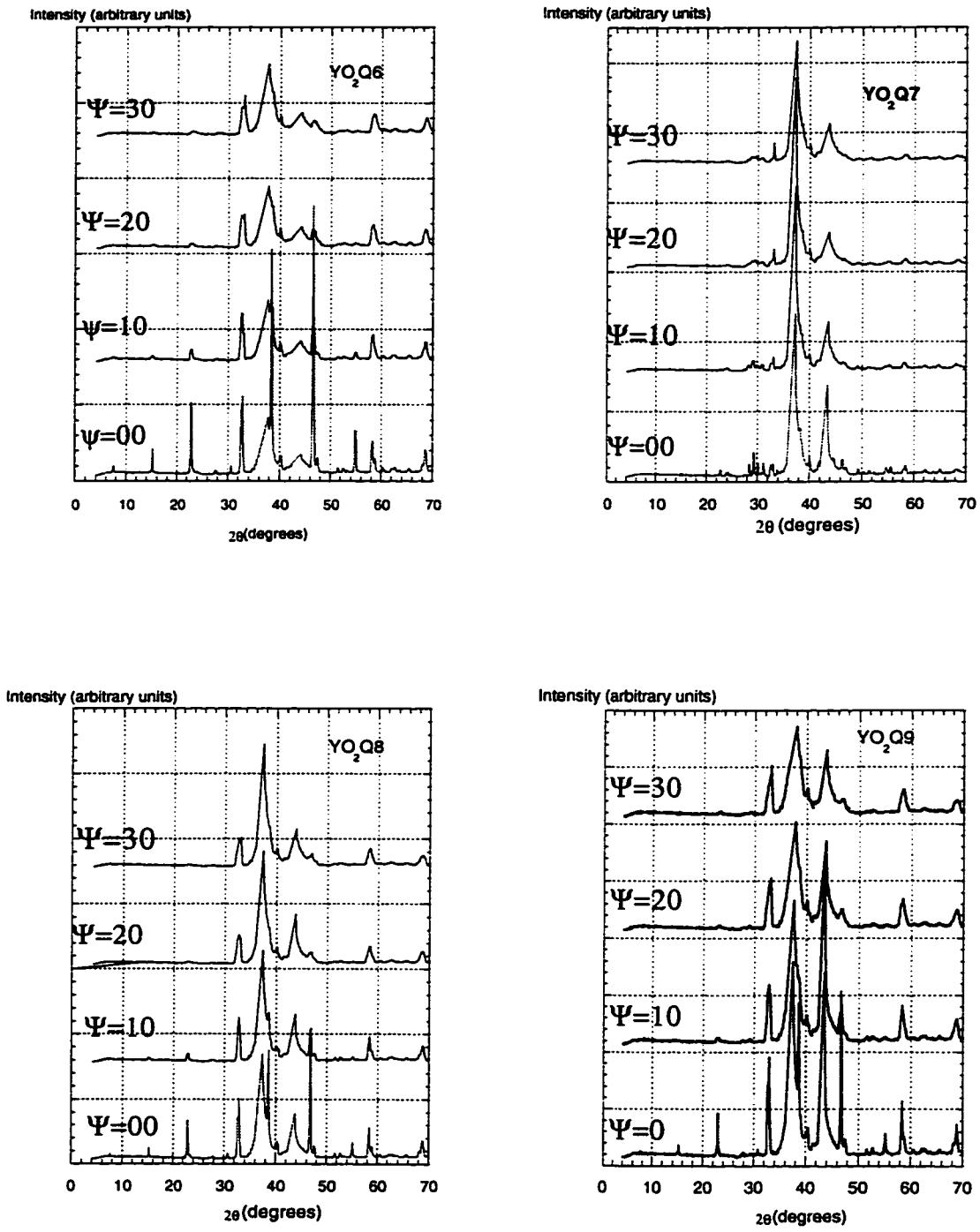

Figure A.3: *Different samples annealed in oxygen gas for different time periods and then quenched to liquid nitrogen refer to table 3.2 for the history of each sample.*

Bibliography

[1] M. M. H. Abdelhadi. Critical currents and pinning forces in ybco hi- tc superconductor. Master's thesis, King Fahd University of Petroleum and Minerals, 1993.

[2] J. G. Bednorz and K. A. Muller. *z. Phys. B*, 64:189–193, 1986.

[3] R. Beyers and T. M. Shaw. *Solid State Physics-Advances in Research and Applications*, 42:135–212, 1989.

[4] G. Burns. *High-Temperature Superconductivity An Introduction.* Academic Press, Inc., Boston, 1992.

[5] M. Cankurtaran. *Supercond. Sci. Technol.*, 6:4–9, 1994.

[6] M. Cankurtaran and G. A. Saunders. *Supercond. Sci. Technol.*, 5:210–215, 1992.

[7] Jr. Timir Datta Charles P. Poole and Horacio A. Farach. *Copper Oxide Superconductors.* John Wiley Sons, New York, 1988.

[8] B. D. Cullity. *Elements of X-ray Diffraction.* Addison-Wesley, Reading, Massachusetts, 1987.

[9] G. Samara D. Saint-James and E. J. Thomas. *Type II Superconductivity.* Pergamon Press, Oxford, 1969.

[10] A. A. Pramana DN. Oxegen stoichiometry effect on magnetic properties of ybco superconductor. Master's thesis, King Fahd University of Petroleum and Minerals, 1995.

[11] J. D. Doss. *Engineering Guide to High-Temperature Superconductivty.* John Wiley Sons, New York, 1989.

[12] A. K. Klehe et al. *Physica C*, 257:105–116, 1996.

[13] A. Schilling et al. *Nature*, 363:56–58, 1993.

[14] C. Namgung et al. *Physica C*, 168:346–350, 1990.

[15] C. W. Chu et al. *Phys. Rev. Lett.*, 58:405, 1987.

[16] C. W. Chu et al. *Nature*, 365:323–325, 1993.

[17] E. D. Specht et al. *Phy. Rev. B*, 37:7426, 1988.

[18] F. Yakhou et al. *Physica C*, 261:315–322, 1996.

[19] J. C. Russ et al., editor. *Advances in X-Ray Analysis*, volume 25, New York, 1982. University of Denver, Plenum Press.

[20] J. D. Jorgensen et al. *Phys. Rev. B*, 41:1863, 1990.

[21] J. E. Greedan et al. *Phys. Rev. B*, 35:8770, 1987.

[22] L. Gao et al. *Physica C*, 213:261–265, 1993.

[23] M. K. Wu et al. *Phys. Rev. Lett.*, 58:908, 1987.

[24] R. J. Cava et al. *Nature*, 329:423–425, 1987.

[25] R. J. Cava et al. *Physica C*, 165:419–433, 1990.

[26] R. J. Wijngaarden et al. *Physica C*, 185-189:787–788, 1991.

[27] R. K. Singh et al. *Phys. Rev. B*, 51:9155, 1995.

[28] T. A. Vanderah et al. *J. Crystal Growth*, 118:385–395, 1992.

[29] U. Welp et al. *Phys. Rev Lett*, 69:2130, 1992.

[30] W. E. Farneth et al. *Solid State Commun*, 66:953–957, 1988.

[31] W. H. Fietz et al. *Physica C*, 235-240:1785–1786, 1994.

[32] Donald M. Ginsberg, editor. *Physical Properties of High Temperature Superconductors I.* World Scientific, Singapore, 1989.

[33] J. B. Goodenough. *Supercond. Sci. Technol.*, 3:26–36, 1990.

[34] L. C. Gupta, editor. *Theoretical and Experimental Approach to High-Tc and Conventional Superconductivity*, New York, 1991. Tata Institute of Fundamental Research, Bombay, Nova Science Publishers.

[35] R. P. Gupta and M. Gupta. *Physica C*, 178:414–420, 1991.

[36] Nasser Hamdan. *Effects of Temperature and Irradiation on The Properties of The Bismuth-Based Superconductors.* PhD thesis, Middle East Technical University, 1993.

[37] J. Lusk J. L. Tallon and M.R. Prestland. *Physica C*, 173:345–351, 1991.

[38] Laurens Jansen. *Physica C*, 173:409–413, 1991.

[39] E. Kaldis, editor. *Materials and Crystallographic Aspects of High-Tc Superconductivity*, Dorecht, 1994. NATO ASI, Kluwer Academic Publishers.

[40] V. Z. Kersin and S. A. Wolf. *Fundamentals of Superconductivity.* Plenum Press, New York, 1990.

[41] N. M. Hamdan KH. A. Ziq and J. Shirokoff. *Supercond. Sci. Technol.*, 7:118–120, 1994.

[42] J. R. Kirtley and Chang C. Tsuei. *Scientific American*, 275(2):50–55, August 1996.

[43] F. Licci and L. Raffo. *Supercond. Sci. Technol.*, 8:245–251, 1995.

[44] Y. Lye and H. Yasuoka, editors. *The Physics and Chemistry of Oxide Superconductors*, Berlin, 1992. ISSP, Springer-Verlag.

[45] E. A. Lynton. *Superconductivity.* Science Paperbacks, London, 1969.

[46] A. Navrotsky M. E. Parks and K. Mocala. *J. Solid. State Chem.*, 79:53–62, 1989.

[47] J. L. Moran-Lopez and I. K. Schuller, editors. *Oxygen Disorder Effects in High-Tc Superconductors*, New York, 1990. Plenum Press.

[48] Kh. A. Ziq N. M. Hamdan and J. Shirokoff. *Physica C*, 235-240:1217–1218, 1994.

[49] T. P. Orlando and K. A. Delin. *Foundations of Applied Superconductivity.* Addison-Wesley Publishing Company, Reading, Massachusetts, 1991.

[50] J. C. Phillips. *Physics of High-TC Superconductors.* Academic Press, Boston, 1989.

[51] A. C. Rose-Innes. *Introduction To Superconductivity.* Pergamon Press, Oxford, 1978.

[52] M. Tinkham. *Introduction to Superconductivity.* McGraw-Hill Book Company, New York, 1975.

[53] Suntao Yang. *Oxegen Disorder Effects in High Temperature Y-Ba-Cu-O Superconductor.* PhD thesis, Universty of Illinois at Chicago, 1992.

[54] K. Yvon and M. Francois. *Z. Phys. B-Condensed Matter*, 76:413–444, 1989.

IMAGE EVALUATION TEST TARGET (QA-3)

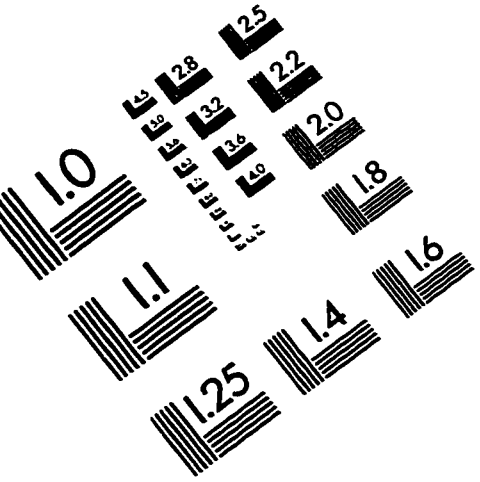

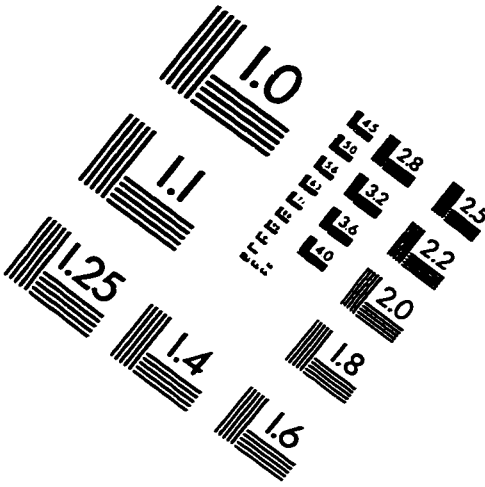

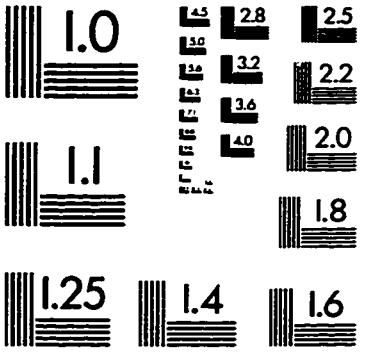

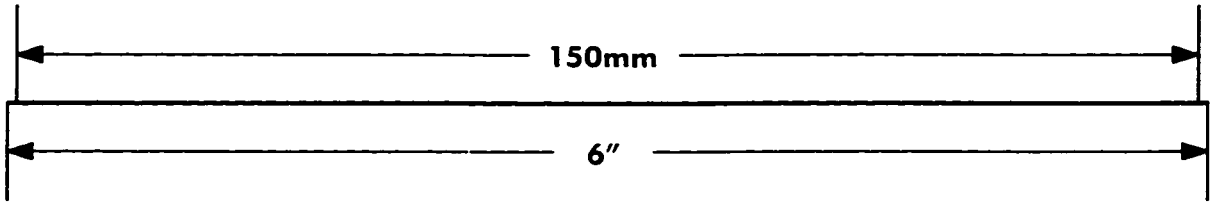

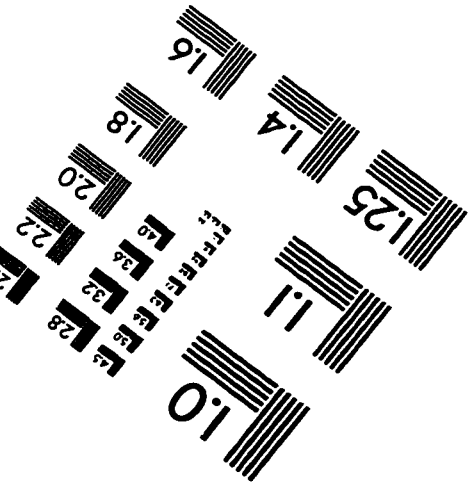

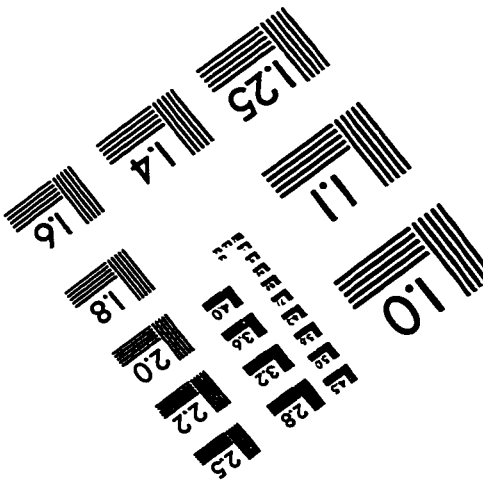

APPLIED IMAGE, Inc
1653 East Main Street
Rochester, NY 14609 USA
Phone: 716/482-0300
Fax: 716/288-5989